

Field-Enhanced Kondo Correlations in a Half-Filling Nanotube Dot: Evolution of an $SU(N)$ Fermi-Liquid Fixed Point

Yoshimichi Teratani,¹ Rui Sakano,² Ryo Fujiwara,³ Tokuro Hata,³
Tomonori Arakawa,³ Meydi Ferrer,^{3,4} Kensuke Kobayashi,³ and Akira Oguri¹

¹*Department of Physics, Osaka City University, Sumiyoshi-ku, Osaka 558-8585, Japan*

²*The Institute for Solid State Physics, the University of Tokyo, Kashiwa, Chiba 277-8581, Japan*

³*Department of Physics, Osaka University, Toyonaka, Osaka 560-0043, Japan*

⁴*Laboratoire de Physique des Solides, CNRS, Université Paris-Sud,
Université Paris Saclay, 91405 Orsay Cedex, France*

(Dated: August 2, 2018)

Carbon nanotube quantum dot has four-fold degenerate one-particle levels, which bring a variety to the Kondo effects taking place in a wide tunable-parameter space. We theoretically study an emergent $SU(2)$ symmetry that is suggested by recent magneto-transport measurements, carried out near two electrons filling. It does not couple with the magnetic field, and emerges in the case where the spin and orbital Zeeman splittings cancel each other out in two of the one-particle levels among four. This situation seems to be realized in the recent experiment. Using the Wilson numerical renormalization group, we show that a crossover from the $SU(4)$ to $SU(2)$ Fermi-liquid behavior occurs as magnetic field increases at two impurity-electrons filling. We also find that the quasiparticles are significantly renormalized as the remaining two one-particle levels move away from the Fermi level and are frozen at high magnetic fields. Furthermore, we consider how the singlet ground state evolves during such a crossover. Specifically, we reexamine the $SU(N)$ Kondo singlet for M impurity-electrons filling in the limit of strong exchange interactions. We find that the nondegenerate Fermi-liquid fixed point of Nozières and Blandin can be described as a bosonic Perron-Frobenius vector for M composite pairs, each of which consists of one impurity-electron and one conduction-hole. This interpretation in terms of the Perron-Frobenius theorem can also be extended to the Fermi-liquid fixed-point without the $SU(N)$ symmetry.

I. INTRODUCTION

Combination of the spin and orbital degrees of freedom causes an interesting variety in the Kondo effects¹ in quantum dots. It arises in various ways, depending on the electron fillings and external fields. For instance, the Kondo states which involve the orbital components such as the ones of the $SU(4)$ and the spin-triplet Kondo effects have been observed as well as the spin-based $SU(2)$ Kondo state.^{2–15} Furthermore, recent ultra-sensitive current and current-noise measurements have precisely identified the Fermi-liquid states with the $SU(2)$ and $SU(4)$ symmetries.¹⁶

In this paper, we focus on electron-correlation effects in a carbon nanotube (CNT) quantum dot^{17,18} with two electrons filling. It is inspired by recent magneto-transport experiment, which observes an unexpected evolution of the Kondo plateau that can be regarded as an indication of a crossover from the $SU(4)$ to $SU(2)$ Fermi-liquid state.¹⁹ As magnetic field increases, the Kondo plateau near half-filling reduces the height from $4e^2/h$ to $2e^2/h$ keeping the flat structure unchanged. This implies that two one-particle levels among the four still remain unlifted near the Fermi level in the magnetic field. This is possible if the magnetic field \vec{B} is applied in such a way that the spin and orbital Zeeman effects cancel each other out.

We study the Kondo effect taking place in this ideal case where the twofold degenerate levels remain near the Fermi level. Using the numerical renormalization group

(NRG),^{20,21} we find that the Kondo correlations are enhanced as magnetic field increases. This is due to the fact that the number of active one-particle levels decreases from four to two, and it makes quantum fluctuations large. Then, we also take into account the perturbations that lift the double degeneracy; specifically the valley mixing, the spin-orbit interaction, and an energy-difference between the spin and orbital Zeeman splittings. We find that the crossover can be seen if the energy gap which is induced by these perturbations is smaller than the Kondo energy scale. For a realistic parameter set deduced from the recent experiments,¹⁹ it is satisfied up to $B \lesssim 5$ T.

One of the other most interesting features of the nanotube dots is that different class of the $SU(N)$ Kondo effects occur depending on the number of electrons M occupying the impurity levels, and such a variation has been observed in recent measurements.¹⁶ In this paper, we also discuss how the ground state evolves as the number electrons M localized in the dot varies. The low-lying energy states of the $SU(N)$ Kondo systems show the Fermi-liquid behavior for any M as Nozières and Blandin mentioned in their well-known paper.²² However, it seems not to be widely recognized how the nondegenerate Fermi-liquid ground state is constructed, for arbitrary occupation number of impurity electrons M , with conduction electrons. Nozières and Blandin considered the limit of a strong exchange interaction $J_K \rightarrow \infty$, at which major effects of electron correlations are determined by the two local sites consisting of the Kondo impurity and one ad-

acent site from the Wilson chain^{20,21} for the conduction band. This limit provides an important information to classify the fixed points of the renormalization group because the effective Kondo-exchange coupling significantly increases at low energies. It was very briefly suggested that the ground state is a non-degenerate singlet which is constructed with M impurity-electrons and $N - M$ conduction electrons in the adjacent site, and this state describes a Fermi-liquid fixed point.²² An explicit derivation of the energy spectrum in this limit, $J_K \rightarrow \infty$, has been given later by Pacollet *et al*, using an $SU(N)$ group-representation theory.²³

In this paper, we also present an alternative interpretation based on a *hole* picture introduced for the conduction electrons. The impurity-electrons and *conduction-holes* with the same *flavor* strongly bind with each other to form M composite pairs. It gives a natural description of the nondegenerate Fermi-liquid fixed point as a bosonic Perron-Frobenius vector, which is a robust and a unique nodeless ground state of M composite hard-core bosons. This description does *not* require the $SU(N)$ symmetry, and thus can be extended to some cases *without* this symmetry.

This paper is organized as follows. We first of all present an interpretation of the Fermi-liquid fixed point for general impurity-electrons filling M in terms of a bosonic Perron-Frobenius vector with and without $SU(N)$ symmetry in the first half of the paper. Then, after these general discussions about the $SU(N)$ Kondo effect, we consider the field-induced crossover from the $SU(4)$ to $SU(2)$ Fermi-liquid behavior observed in recent experiments of a CNT quantum dot¹⁹ in the second half.

In Sec. II, we consider the ground state of $SU(N)$ Anderson and Kondo impurity models to describe a relation between the Fermi-liquid fixed point of Nozières and Blandin and a *totally antisymmetric representation* of the $SU(N)$. In Sec. III, we show that the ground state in the limit of strong Kondo-exchange coupling can be described by a Perron-Frobenius eigenvector for the composite hard-core bosons. Then, in Sec. IV, we introduce a microscopic Hamiltonian \mathbf{H}_d^0 to determine one-particle energy levels of CNT quantum dots, and define a set of renormalized parameters for quasiparticles to describe the Fermi-liquid behavior at low energies. In Sec. V, we show that the field-induced crossover observed in a CNT dot can be explained as a result of a matching of the spin and orbital Zeeman splittings. This matching yields an emergent $SU(2)$ symmetry which does not couple to the magnetic field. We present NRG results for the linear-response conductance and the renormalized parameters for quasiparticles, obtained for the case with this emergent $SU(2)$ symmetry and also for a realistic case where this symmetry becomes only approximate. Summary is given in Sec. VI.

II. $SU(N)$ KONDO EFFECT FOR M IMPURITY-ELECTRONS

We describe the Anderson impurity model for carbon nanotube quantum dots in this section. One of the most significant features of the CNT dot is that different class of the $SU(N)$ Kondo effects can occur depending on the number of electrons M occupying the impurity levels. In this section, we introduce the model to describe CNT dots, and describe how the singlet ground state evolves as the impurity occupation number M varies in the strong-coupling limit, $J_K \rightarrow \infty$, of the $SU(N)$ Kondo model.

A. N -orbital Anderson impurity model for quantum dots

Carbon nanotube quantum dots connected to two leads can be described by an $N (= 4)$ orbital Anderson impurity model: $\mathcal{H} = \mathcal{H}_d + \mathcal{H}_c + \mathcal{H}_T$,

$$\mathcal{H}_d = \sum_{m=1}^N \epsilon_m d_m^\dagger d_m + U \sum_{m < m'} n_{d,m} n_{d,m'}, \quad (1)$$

$$\mathcal{H}_c = \sum_{\nu=L,R} \sum_{m=1}^N \int_{-D}^D d\varepsilon \varepsilon \left(c_{\nu,\varepsilon m}^\dagger c_{\nu,\varepsilon m} - n_c^0(\varepsilon) \right), \quad (2)$$

$$\mathcal{H}_T = \sum_{\nu=L,R} \sum_{m=1}^N v_\nu \left(\psi_{\nu,m}^\dagger d_m + d_m^\dagger \psi_{\nu,m} \right), \quad (3)$$

$$\psi_{\nu,m} \equiv \int_{-D}^D d\varepsilon \sqrt{\rho_c} c_{\nu,\varepsilon m}, \quad n_{d,m} \equiv d_m^\dagger d_m. \quad (4)$$

Here, d_m^\dagger creates an electron with energy ϵ_m in the m -th one-particle level ($m = 1, 2, \dots, N$) of the dot. We also call m the “*flavor*” in the following. In the present study we assume that the Coulomb interaction between whole the electrons occupying the dot can be characterized by a single parameter U . The conduction electrons are described by the operator $c_{\nu,\varepsilon m}^\dagger$ for the lead on the left and right ($\nu = L, R$). It is normalized as $\{c_{\nu,\varepsilon m}, c_{\nu',\varepsilon' m'}^\dagger\} = \delta(\varepsilon - \varepsilon') \delta_{\nu\nu'} \delta_{mm'}$. The Fermi level is situated at the center $\varepsilon_F = 0$ of the conduction band with the width $2D$. For subtracting a constant energy of the conduction electrons filling the noninteracting band, we introduce $n_c^0(\varepsilon) \equiv \Theta(-\varepsilon)$ with $\Theta(\varepsilon)$ the step function. The tunneling matrix element v_ν in Eq. (3) is assumed that it preserves the orbital index m . The resonance energy scale is denoted as $\Delta_\nu \equiv \pi \rho_c v_\nu^2$ with $\rho_c = 1/(2D)$, and $\Delta \equiv \Delta_L + \Delta_R$. Among whole the conduction electron degrees of freedom, only the following linear combination corresponding to the bonding component is coupled to the impurity levels corresponding to the dot. Therefore,

the tunneling Hamiltonian can be expressed such that

$$\mathcal{H}_T = \sum_{m=1}^N v (d_m^\dagger a_m + a_m^\dagger d_m), \quad v \equiv \sqrt{v_L^2 + v_R^2}, \quad (5)$$

$$a_m \equiv \sum_{\nu=L,R} \frac{v_\nu}{v} \psi_{\nu,m}, \quad c_{\epsilon m} \equiv \sum_{\nu=L,R} \frac{v_\nu}{v} c_{\nu,\epsilon m}. \quad (6)$$

For carbon nanotube quantum dots, the one-particle levels with the energy ϵ_m for $m = 1, 2, 3, 4$ consist of the spin (\uparrow, \downarrow) and valley (K, K') degrees of freedom. We will explicitly determine ϵ_m in Sec. IV, using a microscopic one-particle Hamiltonian \mathbf{H}_d^0 which takes into account the spin-orbit interaction, the valley mixing, and spin and orbital Zeeman couplings. In Eq. (1), we have taken the intra- and inter-valley Coulomb repulsions to be identical, and have also neglected Hund's rule coupling J_H . This is consistent with recent measurements for the SU(4) Kondo effect^{16,19} and with previous nanotube data.⁵ Some corrections due to J_H have been found for the ridges other than the SU(4) one, or in other experiments.²⁴ That is, however, beyond the scope of this paper and will be discussed elsewhere. The *flavor* “ m ” conserving tunneling, described by Eqs. (3) and (6), can physically be realized for the leads which are formed in the same nanotube.

The multi-orbital Anderson impurity model \mathcal{H} , defined in Eqs. (1)–(3), has an SU(N) symmetry in the case of $\epsilon_m \equiv \epsilon_d$ for $m = 1, 2, \dots, N$, where all the one-particle energies of impurity levels are identical. It is a rotation symmetry in an N dimensional orbital, or *flavor*, space. The total Hamiltonian \mathcal{H} becomes invariant to transformations by arbitrary unitary matrix $\mathcal{U}_{mm'}$,

$$d'_m = \sum_{m'=1}^M \mathcal{U}_{mm'} d_{m'}, \quad c'_{\nu,\epsilon m} = \sum_{m'=1}^N \mathcal{U}_{mm'} c_{\nu,\epsilon m'}. \quad (7)$$

The SU(N) symmetric Anderson model has intensively been studied, particularly in the limit of large Coulomb interaction $U \rightarrow \infty$ where the average number of impurity-electrons $M = \sum_m \langle d_m^\dagger d_m \rangle$ takes a value in the range $M \leq 1$.^{25–29} Whether or not the system has the SU(N) symmetry does *not* depend on the impurity level-position of ϵ_d , and thus different class of the SU(N) Kondo effects can occur depending on the number of electrons occupying the dot levels M , which varies with the parameters ϵ_d , U , and Δ . For instance, $N = 4$ for CNT dots, and the Fermi-liquid behavior has been observed for $M = 1, 2$, and 3 varying the gate voltage which corresponds to ϵ_d .¹⁶

At half-filling $M = N/2$, which is achieved for the level-position $\epsilon_d = -(N-1)U/2$, the Hamiltonian also has an electron-hole symmetry as well as the SU(N). For this case, perturbation expansion with respect to the Coulomb interaction U has been examined, extending the calculations of Yamada-Yosida for $N = 2$ ^{30,31} to general N .³² The wavefunction renormalization factor Z and the vertex correction $\Gamma_{mm';m'm}(0, 0; 0, 0)$ for $m \neq m'$ have

been calculated up to order U^3 and U^4 , respectively,

$$\frac{1}{Z} = 1 + \left(3 - \frac{\pi^2}{4}\right) (N-1) u^2 - \left(\frac{21}{2}\zeta(3) - 7 - \frac{\pi^2}{2}\right) (N-1)(N-2) u^3 + \dots, \quad (8)$$

$$\begin{aligned} \frac{1}{\pi\Delta} \Gamma_{mm';m'm}(0, 0; 0, 0) = & \\ & u - (N-2)u^2 + \left[N^2 - \left(\frac{\pi^2}{2} - 1\right)N + 9 - \frac{\pi^2}{2}\right] u^3 \\ & - (N-2) \left[N^2 - \left(12 + \frac{7}{4}\pi^2 - 21\zeta(3)\right) N \right. \\ & \left. - 17 - \frac{71}{12}\pi^2 + \frac{133}{2}\zeta(3) \right] u^4 + \dots, \quad (9) \end{aligned}$$

where $u \equiv U/(\pi\Delta)$, and $\zeta(x)$ is the Riemann zeta function. For $N > 2$, both $1/Z$ and $\Gamma_{mm';m'm}(0, 0; 0, 0)$ become *not* even nor odd function of U . These results explicitly show that the power series expansion in U works at least for small U , or small rescaled-coupling $g \equiv (N-1)u$,^{33,34} because the coefficients are finite. Therefore, the ground state can evolve from the non-interacting one through the adiabatic switching-on of U at half-filling. The NRG calculations for the SU(4) Anderson model, carried out in a wide range of the impurity-electron filling $0 < M < 4$ and the Coulomb interaction U or $g \equiv (N-1)u$, also clearly indicate the Fermi-liquid behavior.^{11,12,34,35} We will describe the renormalized parameters for the CNT dots in more detail in Sec. IV.

B. Fermi-liquid fixed point for M impurity-electrons

In order to gain an insight into how the ground state varies with N and M , we next consider a strong-coupling limit, $J_K \rightarrow \infty$, of the SU(N) Kondo model. In this case, the impurity electrons and the *adjacent* conduction electrons which directly couple to the impurity electrons via J_K , are decoupled from the rest of the conduction-electron degrees of freedom. Thus, the Hamiltonian for the impurity and *adjacent* conduction electrons can be described in an N^2 -dimensional Hilbert space, and can be diagonalized. For finite J_K , there are quantitative corrections due to the rest of the conduction-electron degrees of freedom. Nevertheless, the effective Kondo coupling \tilde{J}_K significantly increases at low energies, as it can be expected from the poor-man's scaling theory^{22,36} (see appendix A 3). Therefore, qualitatively, the fixed points of the renormalization group can be classified according to eigenvectors of the two-site model describing the $J_K \rightarrow \infty$ limit.

Nozières and Blandin gave a brief important statement in the footnote 9 of their well-known paper, without providing details.²² It perfectly describes the ground-state wavefunction in the strong exchange-interaction limit:

for general N and M the ground state is a nondegenerate singlet consisting of M impurity-electrons and $N - M$ adjacent conduction electrons a_m . These N electrons are distributed evenly into the one-particle levels with *different* orbital index “ m ”, and this state describes a fixed point with the usual Fermi-liquid behavior. An explicit proof has been provided later by Parcollet *et al*, applying a representation theory to the $SU(N)$ Kondo model.²³ Note that the statement of Nozières and Blandin is based on the Coqblin-Schrieffer form of the exchange interaction,³⁷ which can also be written in the $SU(N)$ Kondo form. We will discuss this singlet state more precisely in this section.

For certain special finite values of the exchange coupling, Affleck has shown that, at half-filling $M = N/2$ for even N , the $SU(N)$ Kondo impurity can be absorbed into that of the orbital, or *flavor*, sector of the conduction electron degrees of freedom, using the non-Abelian bosonization approach.³⁸ For this special case, the Hamiltonian can be diagonalized using the Kac-Moody algebra, and it shows that the excitation spectrum are described by the quasiparticle excitations of the local Fermi liquid. Low-energy Fermi-liquid properties of the $SU(N)$ Kondo model have been also studied away from half-filling,^{39,40} extending Nozières’s description of the local Fermi liquid.⁴¹

1. Coqblin-Schrieffer model vs. $SU(N)$ -Kondo model

To describe the singlet state of Nozières and Blandin in more detail, we consider the case $\Delta \ll U$ where the hybridization energy is much smaller than the Coulomb interaction. Since the eigenvalue of \mathcal{H}_d is $E_M \equiv \varepsilon_d M + UM(M - 1)/2$, the impurity contains M electrons in the atomic limit $v \rightarrow 0$ for

$$-MU < \varepsilon_d < -(M - 1)U. \quad (10)$$

For large Coulomb interactions $U \gg \Delta$, the effective Hamiltonian for the subspace with fixed M impurity-electrons can be obtained through the second-order perturbation in \mathcal{H}_T ,³⁷

$$\mathcal{H}_{\text{eff}} \equiv \mathcal{H}_T \frac{1}{E_M - (\mathcal{H}_d + \mathcal{H}_c)} \mathcal{H}_T \simeq \mathcal{H}_K + \mathcal{H}_{\text{ps}}, \quad (11)$$

$$\mathcal{H}_K \equiv \frac{J_K}{2} \sum_{mm'} \left(a_m^\dagger a_m d_{m'}^\dagger d_m - \frac{1}{N} a_m^\dagger a_m d_{m'}^\dagger d_{m'} \right), \quad (12)$$

$$J_K \equiv 2 \left(\frac{v^2}{E_{M-1} - E_M} + \frac{v^2}{E_{M+1} - E_M} \right) > 0, \quad (13)$$

$$\mathcal{H}_{\text{ps}} \equiv V_{\text{ps}} \sum_m a_m^\dagger a_m, \quad (14)$$

$$V_{\text{ps}} \equiv \frac{v^2}{E_{M-1} - E_M} \frac{M}{N} - \frac{v^2}{E_{M+1} - E_M} \left(1 - \frac{M}{N} \right). \quad (15)$$

The exchange coupling is positive $J_K > 0$, for ε_d given in Eq. (10). We focus on the exchange interaction \mathcal{H}_K

and will omit the potential scattering term \mathcal{H}_{ps} in the following.

Equation (12) is the usual Coqblin-Schrieffer form of the exchange interaction, applicable to general M . It can also be written in the $SU(N)$ Kondo form,^{23,38} using an identity shown in appendix A 1,

$$\mathcal{H}_K = J_K (\mathbf{a}^\dagger \mathbf{T}^\mu \mathbf{a}) (\mathbf{d}^\dagger \mathbf{T}^\mu \mathbf{d}). \quad (16)$$

Here, $\mathbf{a}^\dagger \equiv (a_1^\dagger, \dots, a_N^\dagger)$ is a row vector of the operators. We use the Einstein convention for Greek superscripts, namely the repeated ones are summed. The $SU(N)$ generators \mathbf{T}^μ for $\mu = 1, 2, \dots, N^2 - 1$ are traceless $N \times N$ Hermitian matrices of the *fundamental* representation, satisfying the commutation relations,

$$[\mathbf{T}^\mu, \mathbf{T}^\nu] = i f^{\mu\nu\lambda} \mathbf{T}^\lambda, \quad (17)$$

where $f^{\mu\nu\lambda}$ is the structure factors. Explicit expressions for \mathbf{T}^μ are given in Eqs. (A3)–(A5). The local “spin” $\mathbf{d}^\dagger \mathbf{T}^\mu \mathbf{d}$ for M impurity-electrons can be expressed in terms of the matrices, as shown in appendix A 2:

$$\mathcal{H}_K^{(M)} = J_K (\mathbf{a}^\dagger \mathbf{T}^\mu \mathbf{a}) \mathcal{S}_{r_M}^\mu. \quad (18)$$

Here, a set of the matrices $\mathcal{S}_{r_M}^\mu$ consists a $\binom{N}{M}$ dimensional representation of the $SU(N)$, which we denote r_M , and satisfies the same commutation relations as Eq. (17),

$$[\mathcal{S}_{r_M}^\mu, \mathcal{S}_{r_M}^\nu] = i f^{\mu\nu\lambda} \mathcal{S}_{r_M}^\lambda. \quad (19)$$

The Kondo form of the exchange interaction, Eq. (16) or Eq. (18), makes the symmetric property of the Hamiltonian explicit. For instance, with this Kondo Hamiltonian, the one-loop scaling equation can be calculated simply following along the same line carried out for the $SU(2)$ case, replacing the spin matrices for the conduction and impurity electrons by the $SU(N)$ ones \mathbf{T}^μ and $\mathcal{S}_{r_M}^\mu$, respectively (see appendix A 3). To the one-loop order, the scaling equation does not depend on M as shown in Eq. (A12), but a factor that is proportional to N gives the Kondo temperature of the form $T_K = D \exp[-\frac{2}{N\rho_c J_K}]$.

One thing we would like to emphasize in this section is that a *hole picture*, which we introduce for the conduction electrons such that

$$b_m \equiv a_m^\dagger, \quad h_{\epsilon m} \equiv c_{\epsilon m}^\dagger, \quad (20)$$

keeping the impurity electrons d_m unchanged, becomes a natural description of the singlet ground state for $N > 2$. With these conduction holes, the Hamiltonian Eq. (16) takes the form,

$$\mathcal{H}_K = J_K (\mathbf{b}^\dagger \bar{\mathbf{T}}^\mu \mathbf{b}) (\mathbf{d}^\dagger \mathbf{T}^\mu \mathbf{d}). \quad (21)$$

The matrices $\bar{\mathbf{T}}^\mu \equiv (-\mathbf{T}^\mu)^*$ satisfy the same commutation relations as Eq. (17), namely the *hole picture* correspond to the *conjugate representation* of the $SU(N)$.

We note that the *hole picture* of this form is suitable for $M \leq N/2$. It should be modified in an opposite way for $M > N/2$, applying the electron-hole transformation to the impurity-electrons keeping conduction electrons unchanged. In the following, we assume $0 < M \leq N/2$ since the other case corresponds to the charge conjugate defined with respect to the whole electrons.

2. Singlet state in $J_K \rightarrow \infty$ limit for M impurity-electrons

As the renormalized exchange coupling \tilde{J}_K , defined in Eq. (A12), grows large at low energies, behavior in the strong coupling limit $J_K \rightarrow \infty$ determines the fixed-point of the renormalization group in the first approximation.²⁰ In this limit, the wavefunction is determined by diagonalizing \mathcal{H}_K consisting of the impurity electrons and the adjacent conduction electrons a_m , neglecting \mathcal{H}_c the bulk part of the conduction electrons.

The number of the adjacent conduction holes, $N_b = \sum_m b_m^\dagger b_m$, is conserved in this limit. Therefore, the wavefunction for given M and N_b can be expanded using a direct-product basis set which consists of $\overline{\binom{N}{M}} \otimes \overline{\binom{N}{N_b}}$ states, where the bar on the top of the binomial coefficient for the *holes* is a label assigned for the *conjugate representation*.^{42,43} The Hilbert space can be decomposed into a direct sum of irreducible representations, in a similar way such that the product states of 2 spins are decomposed into $2 \otimes 2 = 1 \oplus 3$ in the SU(2) case. The decomposition for the 2-site SU(N) Kondo model has been carried out by Parcollet *et al* in the electron picture.²³ They showed that a *one-dimensional* representation emerges at $N_b = M$ as a Young tableau of a single column with the *greatest possible number of boxes* N , and it becomes the ground state for $J_K \rightarrow \infty$. This state corresponds to a *totally antisymmetric representation* (TAR), and in our *hole picture* it can be interpreted as

$$\binom{N}{M} \otimes \overline{\binom{N}{M}} = 1 \oplus \dots \quad (22)$$

For example, in the SU(4) case, the product states for $N_b = M$ can be decomposed into $4 \otimes \bar{4} = 1 \oplus 15$ for $M = 1$, and $6 \otimes \bar{6} = 1 \oplus 15 \oplus 20$ for $M = 2$. Note that, at half-filling $M = N/2$ for even N , the conjugate representation for the holes $(-\mathcal{S}_{r_M}^\mu)^*$ becomes equivalent to r_M which is for the electrons $\mathcal{S}_{r_M}^\mu$.

This *nondegenerate singlet* state emerges in the case where the total number of electrons becomes $N = M + N_a$ with $N_a \equiv N - N_b$ the number of adjacent conduction electrons, and can be explicitly expressed in the form

$$|\text{TAR}\rangle_M \equiv \frac{1}{\sqrt{\binom{N}{M}} (N-M)!M!} \times \sum_{\{j\}} \text{sgn}(\{j\}) d_{j_1}^\dagger d_{j_2}^\dagger \cdots d_{j_M}^\dagger a_{j_{M+1}}^\dagger \cdots a_{j_{N-1}}^\dagger a_{j_N}^\dagger |0\rangle. \quad (23)$$

Here, $\{j\} = \{j_1, j_2, \dots, j_N\}$ is a set of N integers $1, 2, \dots, N$, and the summation extends over all the $N!$ permutations with the sign factor $\text{sgn}(\{j\}) = +1$ or -1 being taken according to whether $\{j\}$ is even or odd. This wavefunction can also be rewritten in a totally symmetric form in terms of the *conduction holes* through a simple rearrangement of the conduction-electron operators,

$$|\text{TAR}\rangle_M \equiv \frac{1}{\sqrt{\binom{N}{M}}} \sum_{j_1 < j_2 < \cdots < j_M} d_{j_1}^\dagger a_{j_1} d_{j_2}^\dagger a_{j_2} \cdots d_{j_M}^\dagger a_{j_M} |\tilde{0}\rangle, \quad (24)$$

where $|\tilde{0}\rangle \equiv a_1^\dagger a_2^\dagger \cdots a_N^\dagger |0\rangle$. It can also be interpreted as a bosonic wavefunction for the particle-hole pairs $d_j^\dagger a_j$. The TAR truly corresponds to the singlet ground state that Nozières and Blandin mentioned.^{22,23} For finite J_K , this state evolves to a Kondo singlet, involving low-energy conduction electrons far away from the impurity site. Successive inclusion of such conduction electrons can be carried out with the NRG, and the low-lying excitations show the SU(N) Fermi-liquid behavior.

III. FERMI-LIQUID FIXED POINT AS A BOSONIC PERRON-FROBENIUS VECTOR

We describe more precisely the interpretation of the TAR in terms of a *hard-core boson*, which is a composite particle consisting of one impurity-electron and one adjacent conduction-hole with the same *flavor* “ m ” appearing in Eq. (24). With a basis set of the hard-core bosons, all the off-diagonal elements of the Hamiltonian becomes *non-positive*, for which the Perron-Frobenius theorem is applicable. It clearly explains why the TAR becomes the *unique* lowest-energy state that can be written as a *nodeless bosonic* wavefunction in the form of Eq. (24). This description does *not* require the SU(N) symmetry, and the Perron-Frobenius ground state remains robust against perturbations which break the SU(N) symmetry as long as the off-diagonal elements of the Hamiltonian can be kept *non-positive*.

A. Hard-core bosons in the SU(N) symmetric case

The discussions given in Sec. IIB2 were based on a group-representation description of the SU(N). In order to gain physical insights into the nondegenerate state, we now go back to the Coqblin-Shrieffer form, but with the *hole picture* using Eq. (20),

$$\mathcal{H}_K = \frac{J_K}{2} \left(- \sum_{mm'} d_{m'}^\dagger b_{m'}^\dagger b_m d_m + \frac{1}{N} \sum_{mm'} b_m^\dagger b_m d_m^\dagger d_{m'} \right). \quad (25)$$

For $J_K \rightarrow \infty$, the second term in the bracket becomes a constant $N_b M/N$, taking the summation over m and m' .

The first term can be interpreted as a *tunneling* Hamiltonian for the composite hard-core bosons, $Q_m \equiv b_m d_m$ and $Q_m^2 = 0$, which consists of one impurity-electron and one conduction-hole of the same flavor “ m ”. This Hamiltonian is also equivalent to a reduced BCS model, for which exact solution was obtained by Richardson⁴⁴ in the context of nuclear physics, and it was also applied to ultra-small-grain superconductors by von Delft and Braun.⁴⁵ We apply the same approach to the ground state of Eq. (25) for M impurity-electrons filling.

In our case, the hard-core bosons can *hop* around, via the matrix element J_K , onto the vacant orbitals, which are *not* occupied by other hard-core bosons nor the immobile unpaired objects such as a singly-occupied impurity-electron and a singly-occupied conduction-hole. The number of the composite pairs N_{pair} is conserved. Similarly, the number of unpaired impurity-electrons $N_{\mathcal{O}_d} = M - N_{\text{pair}}$ and that of the unpaired conduction-holes $N_{\mathcal{O}_h} = N_b - N_{\text{pair}}$ are also conserved. Thus, the number of the *unblocked* orbitals which are *not* occupied by these unpaired objects becomes $N_{\mathcal{UB}} \equiv N - N_{\mathcal{O}_d} - N_{\mathcal{O}_h} = N - M - N_b + 2N_{\text{pair}}$. Symbolically, \mathcal{O}_d and \mathcal{O}_h denote a set of orbitals occupied by the unpaired impurity-electrons and unpaired conduction-holes, respectively, while \mathcal{UB} denotes a set of *unblocked* orbitals.⁴⁵ Taking N_{pair} as a quantum number, the eigenstates can be expanded in the form

$$|N_{\text{pair}}; \{m_h\}, \{m_d\}\rangle \equiv \prod_{m_h \in \mathcal{O}_h} b_{m_h}^\dagger \prod_{m_d \in \mathcal{O}_d} d_{m_d}^\dagger |\Psi_{\text{pair}}\rangle, \quad (26)$$

$$|\Psi_{\text{pair}}\rangle = \sum_{j_1 < \dots < j_{N_{\text{pair}}} \in \mathcal{UB}} \psi_{\text{pair}}(j_1, \dots, j_{N_{\text{pair}}}) Q_{j_1}^\dagger Q_{j_2}^\dagger \dots Q_{j_{N_{\text{pair}}}}^\dagger |\tilde{0}\rangle. \quad (27)$$

The level indices $\{m_h\} = \{m_{h,1}, \dots, m_{h,N_{\mathcal{O}_h}}\}$ and $\{m_d\} = \{m_{d,1}, \dots, m_{d,N_{\mathcal{O}_d}}\}$ for the unpaired objects can also be regarded as quantum numbers. The vacuum for the conduction holes is defined such that $b_j |\tilde{0}\rangle = 0$ and $d_j |\tilde{0}\rangle = 0$. The configuration of these unpaired objects does not affect the energy while it causes the degeneracy $g_{M,N_b,N_{\text{pair}}}$ of the eigenstates,

$$g_{M,N_b,N_{\text{pair}}} = \frac{N!}{(M - N_{\text{pair}})! (N_b - N_{\text{pair}})! N_{\mathcal{UB}}!}. \quad (28)$$

In Eq. (27), the summation for each of j 's runs over *unblocked* orbitals with a requirement $j_1 < \dots < j_{N_{\text{pair}}}$. The pair wavefunction $\psi_{\text{pair}}(j_1, \dots, j_{N_{\text{pair}}})$ is determined by the Schrödinger equation $\mathcal{H}_K |\Psi_{\text{pair}}\rangle = \epsilon |\Psi_{\text{pair}}\rangle$, which describes the self-avoiding motion of the N_{pair} hard-core bosons onto the $N_{\mathcal{UB}}$ vacant orbitals. With this basis set, the Hamiltonian for the pairs is written as a $\binom{N_{\mathcal{UB}}}{N_{\text{pair}}}$ dimensional matrix. It has $(N_{\mathcal{UB}} - N_{\text{pair}}) N_{\text{pair}}$ non-zero off-diagonal elements in each row, and in each column, as the total number of the allowed *hopping* processes is given by product of the number of vacant orbitals

and the number of pairs. Furthermore, all such non-zero off-diagonal elements take the same negative value $-J_K/2 < 0$ owing to the bosonic commutation relation between the two different pairs. To those matrices of this form, the Perron-Frobenius theorem is applicable since the *connectivity* condition necessary for this theorem also holds for the *pair hopping* in this $\binom{N_{\mathcal{UB}}}{N_{\text{pair}}}$ dimensional space. The Perron-Frobenius theorem states that the lowest-energy state becomes nondegenerate and has a nodeless eigenvector,⁴⁶ which in our case is a uniform $\binom{N_{\mathcal{UB}}}{N_{\text{pair}}}$ dimensional vector. Thus, the lowest energy state in each subspace labeled by the quantum number $(M, N_b, N_{\text{pair}})$ can be explicitly written in the form,

$$\psi_{\text{pair}}^{\text{min}}(j_1, \dots, j_{N_{\text{pair}}}) = \frac{1}{\sqrt{\binom{N_{\mathcal{UB}}}{N_{\text{pair}}}}}, \quad (29)$$

$$\epsilon_{M,N_b,N_{\text{pair}}}^{\text{min}} = \frac{J_K}{2} \left[-(N_{\mathcal{UB}} - N_{\text{pair}} + 1) N_{\text{pair}} + \frac{N_b M}{N} \right]. \quad (30)$$

It takes the absolute minimum at $N_b = N_{\text{pair}} = M$, where all the orbitals are *unblocked* $N_{\mathcal{UB}} = N$. Thus, the ground state is nondegenerate and is identical to the TAR, given in Eqs. (23) and (24),

$$\epsilon_M^{\text{GS}} = -J_K \frac{M(N-M)(N+1)}{2N}, \quad (31)$$

$$|\Psi\rangle_M^{\text{GS}} = \frac{1}{\sqrt{\binom{N}{M}}} \frac{1}{M!} \left[\sum_{m=1}^N d_m^\dagger b_m^\dagger \right]^M |\tilde{0}\rangle. \quad (32)$$

The energy can also be expressed in terms of the Casimir operator, defined in appendix A 2, as $\epsilon_M^{\text{GS}} = -J_K C_2(r_M)$. It reproduces the result of Pacollet *et al.*,²³ which is obtained using an addition rule for the $\text{SU}(N)$ flavors of the impurity and conduction electrons.^{42,43}

The wavefunction $|\Psi\rangle_M^{\text{GS}}$ describes how the pairs distribute in the *flavor* space. For example, in the $\text{SU}(2)$ case, it takes the form

$$|\Psi\rangle_{M=1}^{N=2} = \frac{1}{\sqrt{2}} \left(d_1^\dagger b_1^\dagger + d_2^\dagger b_2^\dagger \right) |\tilde{0}\rangle \quad (33)$$

$$= \frac{1}{\sqrt{2}} \left(d_1^\dagger a_2^\dagger - d_2^\dagger a_1^\dagger \right) |0\rangle,$$

since $|\tilde{0}\rangle = a_1^\dagger a_2^\dagger |0\rangle$ for $N = 2$. Our main interest is in the $\text{SU}(4)$ symmetric CNT quantum dots, for which the ground state for $M = 1$ and that for $M = 2$ in the $J_K \rightarrow \infty$ limit are given, respectively, by

$$|\Psi\rangle_{M=1}^{N=4} = \frac{1}{2} \left(d_1^\dagger b_1^\dagger + d_2^\dagger b_2^\dagger + d_3^\dagger b_3^\dagger + d_4^\dagger b_4^\dagger \right) |\tilde{0}\rangle, \quad (34)$$

$$|\Psi\rangle_{M=2}^{N=4} = \frac{1}{\sqrt{6}} \left(d_1^\dagger b_1^\dagger d_2^\dagger b_2^\dagger + d_1^\dagger b_1^\dagger d_3^\dagger b_3^\dagger + d_1^\dagger b_1^\dagger d_4^\dagger b_4^\dagger \right. \\ \left. + d_2^\dagger b_2^\dagger d_3^\dagger b_3^\dagger + d_2^\dagger b_2^\dagger d_4^\dagger b_4^\dagger + d_3^\dagger b_3^\dagger d_4^\dagger b_4^\dagger \right) |\tilde{0}\rangle. \quad (35)$$

$$\begin{aligned}
|\Psi\rangle_{N=2, M=1} &= 2 \begin{array}{c} d^\dagger \quad b^\dagger \\ \bullet \quad \circ \\ 1 \end{array} + 2 \begin{array}{c} d^\dagger \quad b^\dagger \\ \quad \quad \\ 1 \end{array} \\
|\Psi\rangle_{N=4, M=1} &= 4 \begin{array}{c} d^\dagger \quad b^\dagger \\ \bullet \quad \circ \\ 3 \\ \quad \quad \\ 2 \\ \quad \quad \\ 1 \end{array} + 3 \begin{array}{c} d^\dagger \quad b^\dagger \\ \bullet \quad \circ \\ 3 \\ \quad \quad \\ 2 \\ \quad \quad \\ 1 \end{array} + 3 \begin{array}{c} d^\dagger \quad b^\dagger \\ \quad \quad \\ 3 \\ \bullet \quad \circ \\ 2 \\ \quad \quad \\ 1 \end{array} + 3 \begin{array}{c} d^\dagger \quad b^\dagger \\ \quad \quad \\ 3 \\ \quad \quad \\ 2 \\ \bullet \quad \circ \\ 1 \end{array} \\
|\Psi\rangle_{N=4, M=2} &= 4 \begin{array}{c} d^\dagger \quad b^\dagger \\ \bullet \quad \circ \\ 3 \\ \bullet \quad \circ \\ 2 \\ \quad \quad \\ 1 \end{array} + 3 \begin{array}{c} d^\dagger \quad b^\dagger \\ \bullet \quad \circ \\ 3 \\ \quad \quad \\ 2 \\ \bullet \quad \circ \\ 1 \end{array} + 3 \begin{array}{c} d^\dagger \quad b^\dagger \\ \bullet \quad \circ \\ 3 \\ \quad \quad \\ 2 \\ \bullet \quad \circ \\ 1 \end{array} + 3 \begin{array}{c} d^\dagger \quad b^\dagger \\ \quad \quad \\ 3 \\ \bullet \quad \circ \\ 2 \\ \bullet \quad \circ \\ 1 \end{array} + 3 \begin{array}{c} d^\dagger \quad b^\dagger \\ \quad \quad \\ 3 \\ \bullet \quad \circ \\ 2 \\ \bullet \quad \circ \\ 1 \end{array} + 3 \begin{array}{c} d^\dagger \quad b^\dagger \\ \quad \quad \\ 3 \\ \quad \quad \\ 2 \\ \bullet \quad \circ \\ 1 \end{array}
\end{aligned}$$

FIG. 1. Schematic picture of the nondegenerate singlet ground state of the SU(4) Kondo model with $M = 1$ and $M = 2$ impurity-electrons in the limit of $J_K \rightarrow \infty$. The wavefunction for the SU(2) case with $M = 1$ is also illustrated on the top for comparison. Each row represents *flavor* “ m ” of the levels $m = 1, 2, 3, 4$. The first (d^\dagger) and second (b^\dagger) columns represent orbitals in the impurity and the adjacent conduction site, respectively, with (\bullet) the impurity-electrons and (\circ) the conduction-holes. The explicit expressions for these states are given in Eqs. (34) and (35), respectively.

In Fig. 1, the configuration of the electrons and holes in the ground state of these cases are schematically illustrated. Each of M composite electron-hole pairs is in the same row labeled by the *flavor* “ m ”. These pairs are uniformly distributed along the vertical direction in the N different rows, constructing a nondegenerate wavefunction as a nodeless linear combination in which all the coefficients are identical. This agrees with the statement of Nozières and Blandin stated given in the footnote 9 of their paper,²² namely the singlet ground state for M impurity electrons is constructed with $N - M$ adjacent conduction electrons.

The charge distribution of this form can also be understood from an Anderson-impurity point of view. Suppose the situation where $U = 0$ and $\varepsilon_d \ll -\Delta$. The noninteracting ground state is nondegenerate, and the

impurity site is almost full filled by N electrons. If the Coulomb repulsion U is switched on gradually keeping the level position ε_d unchanged, the number of impurity-electrons will decrease as the ground state evolves continuously. At a certain value of U , the average number of impurity-electrons becomes M and the phase shift becomes $\delta = \pi M/N$ as totally $N - M$ electrons have already moved towards the conduction band.

For finite exchange interaction J_K , the wavefunction $|\Psi\rangle_M^{\text{GS}}$ evolves to the Kondo singlet state which shows the SU(N) Fermi-liquid behavior. There is also an interesting analogy with the SU(N) gauge theory, in which the TAR corresponding to Fig. 1 describes a M -meson state that is constructed from the quarks (\bullet) and anti-quarks (\circ).^{42,43}

B. Singlet ground state without SU(N) symmetry

We next discuss an evolution of the nondegenerate ground state of Nozières and Blandin in the case without the SU(N) symmetry. In the hard-core boson interpretation mentioned in the above, the singlet state corresponds to the Perron-Frobenius eigenvector, which is a linear-combination of all the basis vectors with strictly *positive* coefficients.⁴⁶ Specifically, in the SU(N) symmetric case, all the coefficients are identical, or *uniform*, as seen in Eq. (29). For some perturbations which breaks the SU(N) symmetry, the Perron-Frobenius eigenvector

can continuously evolve to a vector with *non-uniform* coefficients preserving the *nodeless* structure.

In order to given an explicit example, we examine the case where each of the one-particle energies ϵ_m takes a certain value bounded in the range $\delta\epsilon$ near the middle of the M -electron region defined in Eq. (10),

$$\epsilon_m = -\left(M - \frac{1}{2}\right)U + \delta\epsilon_m, \quad -\frac{\delta\epsilon}{2} < \delta\epsilon_m < \frac{\delta\epsilon}{2}. \quad (36)$$

Specifically, we only take into account an extended exchange-interaction term derived for this case, neglecting the potential scattering term. Details for this

anisotropic exchange coupling, $\mathcal{H}_K^{\text{ais}}$, are described in appendix B.

The fixed-point Hamiltonian in the strong exchange interaction limit can be deduced from $\mathcal{H}_K^{\text{ais}} + \mathcal{H}_d$, which can be expressed in the *hole-picture*, as

$$\begin{aligned} \mathcal{H}_K^{\text{ais}} + \mathcal{H}_d = & \\ & \sum_{m \neq m'} \sum_{\{\alpha\}} -\frac{J_{m'm}^{\{\alpha\}}}{2} d_{m'}^\dagger b_{m'}^\dagger b_m d_m |\{\alpha\}\rangle_{MM} \langle\{\alpha\}| \\ & + \sum_m \sum_{\{\alpha\}} \frac{J_{mm}^{\{\alpha\}}}{2} (1 - b_m^\dagger b_m) d_m^\dagger d_m |\{\alpha\}\rangle_{MM} \langle\{\alpha\}| \\ & - \frac{\bar{J}M(N - N_b)}{2N} + \sum_{\{\alpha\}} E_M^{\{\alpha\}} |\{\alpha\}\rangle_{MM} \langle\{\alpha\}| \end{aligned} \quad (37)$$

Here, $J_{m'm}^{\{\alpha\}}$ and \bar{J} are defined in Eqs. (B3) and (B4), respectively. The exchange coupling $J_{m'm}^{\{\alpha\}}$ becomes anisotropic and depends on the energy of initial and final M impurity-electrons states. The couplings are positive, $J_{m'm}^{\{\alpha\}} > 0$ and $\bar{J} > 0$, for all m, m' , and $\{\alpha\}$ for large Coulomb interactions $U/2 \gg (M + 1/2)\delta\epsilon$, as shown in Eq. (B10). The diagonal elements, which correspond to the last terms in the right-hand side of Eqs. (37), depend also on the distribution of unpaired impurity-electrons $\{m_d\}$ as well as the energy of the initial state $E_M^{\{\alpha\}}$. These are the main differences from the $SU(N)$ symmetric case.

The off-diagonal elements of $J_{m'm}^{\{\alpha\}}$ can also be regarded as the *hopping* matrix elements for the hard-core bosons $Q_m^\dagger \equiv d_m^\dagger b_m^\dagger$ as those in the $SU(N)$ case. The unpaired particles cannot *hop* around the *flavor* space also for this anisotropic case. Therefore, the number of unpaired impurity-electrons $N_{\mathcal{O}_d}$ and that of unpaired conduction-holes $N_{\mathcal{O}_h}$ are conserved, taking values in the range: $N_{\mathcal{O}_d} = 0, 1, \dots, M$, and $N_{\mathcal{O}_h} = 0, 1, \dots, N - M$. Similarly, the numbers $N_b = M - N_{\mathcal{O}_d} + N_{\mathcal{O}_h}$, $N_{\text{pair}} = M - N_{\mathcal{O}_d}$, and $N_{UB} = N - N_{\mathcal{O}_d} - N_{\mathcal{O}_h}$ are also conserved.

Therefore, the eigenstates of $\mathcal{H}_K^{\text{ais}} + \mathcal{H}_d$ can also be expanded using the same basis set as Eqs. (26) and (27):

$$\begin{aligned} & |\{m_p\}; \{m_h\}, \{m_d\}\rangle \\ & \equiv \prod_{m_h \in \mathcal{O}_h} b_{m_h}^\dagger \prod_{m_d \in \mathcal{O}_d} d_{m_d}^\dagger \prod_{m_p \in \text{pairs}} Q_{m_p}^\dagger |\tilde{0}\rangle \end{aligned} \quad (38)$$

$$= \prod_{i=1}^{N_b} b_{\beta_i}^\dagger \prod_{j=1}^M d_{\alpha_j}^\dagger |\tilde{0}\rangle. \quad (39)$$

Here, $\{\alpha_1, \alpha_2, \dots, \alpha_M\}$ and $\{\beta_1, \beta_2, \dots, \beta_{N_b}\}$ represent a set of occupied impurity-electron levels and that of occupied conduction-hole levels, respectively, which we symbolically write $\{\alpha\} = \{m_d\} + \{m_p\}$ and $\{\beta\} = \{m_h\} + \{m_p\}$ as sums of the unpaired and paired elements. The coordinates of the unpaired objects $\{m_h\}$ and $\{m_d\}$ can be regarded as quantum numbers whereas

the coordinates of the pairs $\{m_p\} = \{m_{p,1}, \dots, m_{p,N_{\text{pair}}}\}$ constitute a $\binom{N_{UB}}{N_{\text{pair}}}$ dimensional subspace for the pair wavefunction $\psi_{\text{pair}}(m_{p,1}, \dots, m_{p,N_{\text{pair}}})$.

In the representation using the basis set Eq. (38), the off-diagonal elements of the Hamiltonian matrix become *negative* or zero: there emerge $(N_{UB} - N_{\text{pair}}) N_{\text{pair}}$ *negative* off-diagonal elements $-J_{m'm}^{\{\alpha\}}/2$ in each column, and their Hermitian-conjugate elements emerge in each row. Therefore, similarly to the $SU(N)$ symmetric case, the lowest energy state in each subspace is given by the Perron-Frobenius vector, and all the coefficients which correspond to the pair wavefunction become *positive* $\psi_{\text{pair}}(m_1, \dots, m_{N_{\text{pair}}}) > 0$. However, the coefficients are *not* uniform in the anisotropic case.

The ground state corresponds to the Perron-Frobenius vector for the subspace of $N_{\mathcal{O}_h} = N_{\mathcal{O}_d} = 0$, where all the impurity-electrons and conduction-holes form the pairs, for $U/2 \gg (M + 1/2)\delta\epsilon$ as discussed in appendix B.2. Thus, the ground state for Eq. (37) is also a nondegenerate singlet which is constructed with the M hard-core bosons,

$$|\Psi\rangle_M^{\text{GS}} = \sum_{\{m\}}' \psi_{\text{pair}}^{\text{GS}}(m_1, \dots, m_M) Q_{m_1}^\dagger Q_{m_2}^\dagger \cdots Q_{m_M}^\dagger |\tilde{0}\rangle. \quad (40)$$

Here, each component of $\{m\} = \{m_1, m_2, \dots, m_M\}$ is summed over 1 to N with the constraint: $m_1 < \dots < m_M$. Alternatively, it can also be symmetrized using the properties of the hard-core bosons: $Q_m^2 = 0$ and $[Q_m, Q_{m'}^\dagger] = 0$ for $m \neq m'$. The pair wavefunction is nodeless $\psi_{\text{pair}}^{\text{GS}}(m_1, \dots, m_M) > 0$ but is *not* a uniform function in the case without the $SU(N)$ symmetry. It evolves further for finite exchange couplings $J_{mm}^{\{\alpha\}}$, and will describe the fixed point with the Fermi-liquid behavior.

IV. FERMI-LIQUID THEORY FOR CNT DOTS

A. One-particle Hamiltonian for CNT dots

The one-particle energy levels of the carbon nanotube quantum dots with the energy ϵ_m ($m = 1, 2, 3, 4$) consist of the spin (\uparrow, \downarrow) and valley (K, K') degrees of freedom. Owing to the cylindrical geometry of the CNT, the valley degrees of freedom capture a magnetic moment along the direction of the CNT axis, and it couples to an external magnetic field parallel to the axis.^{13,14,17} Furthermore, the four levels are coupled each other through the spin-orbit interaction Δ_{SO} and valley mixing $\Delta_{KK'}$ term. The one-particle energy ϵ_m is determined as an eigenvalue of the following 4×4 matrix \mathbf{H}_d^0 , which includes these couplings.^{13,14,17} Using a basis set consisting of the spin (\uparrow, \downarrow) and the valley pseudo spin (K, K'), which can be described by the operators $\psi_d^\dagger \equiv (\psi_{K\uparrow}^\dagger, \psi_{K\downarrow}^\dagger, \psi_{K'\uparrow}^\dagger, \psi_{K'\downarrow}^\dagger)$,

the one-particle part of the CNT-dot Hamiltonian can be written in the form,

$$\mathcal{H}_d^0 \equiv \psi_d^\dagger \mathbf{H}_d^0 \psi_d = \sum_m \epsilon_m d_m^\dagger d_m, \quad (41)$$

$$\mathbf{H}_d^0 = \varepsilon_d \mathbf{1}_s \otimes \mathbf{1}_{\text{orb}} + \frac{\Delta_{\text{KK}'}}{2} \mathbf{1}_s \otimes \boldsymbol{\tau}^x + \frac{\Delta_{\text{SO}}}{2} \boldsymbol{\sigma}^z \otimes \boldsymbol{\tau}^z - \vec{\mathcal{M}} \cdot \vec{b}, \quad (42)$$

$$\vec{\mathcal{M}} \equiv -\frac{1}{2} g_s \vec{\boldsymbol{\sigma}} \otimes \mathbf{1}_{\text{orb}} - g_{\text{orb}} \mathbf{1}_s \otimes \boldsymbol{\tau}^z \vec{e}_z. \quad (43)$$

Here, $\boldsymbol{\sigma}^j$ and $\boldsymbol{\tau}^j$ for $j = x, y, z$ are the Pauli matrices for the spin and the valley pseudo-spin spaces, respectively. The Zeeman splitting is determined by the total magnetization $\vec{\mathcal{M}}$, for which $g_s = 2$ and g_{orb} are the g-factors for the spin and valley magnetic moments, respectively, $\vec{b} \equiv \mu_B \vec{B}$ is the external magnetic field with μ_B the Bohr

magneton, and \vec{e}_z is a unit vector along the nanotube axis. In Eq. (42), the SU(4) invariant component ε_d , which can be tuned through the applied gate voltage, is also included in the diagonal part with the unit matrices $\mathbf{1}_s$ and $\mathbf{1}_{\text{orb}}$.

The unitary transform \mathbf{U}_d to diagonalize \mathbf{H}_d^0 , the eigenvalue ϵ_m and the eigenvector \mathbf{u}_m are defined such that

$$\mathbf{H}_d^0 \mathbf{u}_m = \epsilon_m \mathbf{u}_m, \quad \mathbf{u}_m^\dagger \cdot \mathbf{u}_{m'} = \delta_{mm'}, \quad (44)$$

$$\mathbf{d}^\dagger \equiv \psi_d^\dagger \mathbf{U}_d, \quad \mathbf{U}_d = (\mathbf{u}_1, \mathbf{u}_2, \mathbf{u}_3, \mathbf{u}_4). \quad (45)$$

Here, $\mathbf{d}^\dagger = (d_1^\dagger, d_2^\dagger, d_3^\dagger, d_4^\dagger)$, and we will assign the label $m = 1, 2, 3, 4$ such that $\epsilon_1 \leq \epsilon_2 \leq \epsilon_3 \leq \epsilon_4$ unless otherwise noted. We also note that the matrix \mathbf{H}_d^0 can also be expressed in the following 4×4 matrix form: for $\vec{b} = b_{\parallel} \vec{e}_z + b_{\perp} \vec{e}_x$ with $b_{\parallel} \equiv b \cos \Theta$, $b_{\perp} \equiv b \sin \Theta$, and Θ the angle of the magnetic field relative to the nanotube axis,

$$\mathbf{H}_d^0 = \begin{bmatrix} \varepsilon_d + \frac{\Delta_{\text{SO}}}{2} + (g_{\text{orb}} + \frac{g_s}{2}) b_{\parallel} & \frac{g_s}{2} b_{\perp} & \frac{\Delta_{\text{KK}'}}{2} & 0 \\ \frac{g_s}{2} b_{\perp} & \varepsilon_d - \frac{\Delta_{\text{SO}}}{2} + (g_{\text{orb}} - \frac{g_s}{2}) b_{\parallel} & 0 & \frac{\Delta_{\text{KK}'}}{2} \\ \frac{\Delta_{\text{KK}'}}{2} & 0 & \varepsilon_d - \frac{\Delta_{\text{SO}}}{2} - (g_{\text{orb}} - \frac{g_s}{2}) b_{\parallel} & \frac{g_s}{2} b_{\perp} \\ 0 & \frac{\Delta_{\text{KK}'}}{2} & \frac{g_s}{2} b_{\perp} & \varepsilon_d + \frac{\Delta_{\text{SO}}}{2} - (g_{\text{orb}} + \frac{g_s}{2}) b_{\parallel} \end{bmatrix}. \quad (46)$$

B. Renormalized parameters for quasiparticles

Low-energy Fermi-liquid behavior of the Anderson impurity, \mathcal{H} , can be explored using the the Matsubara imaginary-frequency Green's function,^{30,31,41,47-49}

$$\begin{aligned} G_m(i\omega) &\equiv - \int_0^{1/T} d\tau e^{i\omega\tau} \langle T_{\tau} d_m(\tau) d_m^\dagger \rangle \\ &= \frac{1}{i\omega - \epsilon_m - \Sigma_m(i\omega) + i\Delta \text{sgn} \omega}. \end{aligned} \quad (47)$$

Here, $\langle \mathcal{O} \rangle \equiv \text{Tr} [\mathcal{O} e^{-\mathcal{H}/T}] / \text{Tr} [e^{-\mathcal{H}/T}]$ denotes the thermal average. In the following, we consider the zero-temperature limit $T \rightarrow 0$, where the Matsubara frequency ω can be treated as a continuous variable. Behavior of the self energy $\Sigma_m(i\omega)$ near the Fermi level $\omega \simeq 0$ determines the characteristics of the quasiparticles,

$$G_m(i\omega) \simeq \frac{Z_m}{i\omega - \tilde{\epsilon}_m + i\tilde{\Delta}_m \text{sgn} \omega}. \quad (48)$$

The renormalized resonance width $\tilde{\Delta}_m \equiv Z_m \Delta$ and the peak position $\tilde{\epsilon}_m \equiv Z_m [\epsilon_m + \Sigma_m(0)]$ of the local level are parameterized by the wavefunction renormalization factor

$$\frac{1}{Z_m} \equiv 1 - \left. \frac{\partial \Sigma_m(i\omega)}{\partial i\omega} \right|_{\omega=0}. \quad (49)$$

The width of the level m closest to the Fermi level determines the Kondo energy scale $T_K \sim \tilde{\Delta}_m$.

The phase shift, which is defined as the argument of $G_m(i0^+) = -|G_m(i0^+)| e^{i\delta_m}$ in the complex plane, plays an very important role on the ground-state properties. At zero temperature, it determines the occupation number of the local level through the Friedel sum rule

$$\langle n_{d,m} \rangle = \frac{\delta_m}{\pi}, \quad \cot \delta_m = \frac{\epsilon_m + \Sigma_m(0)}{\Delta}. \quad (50)$$

Furthermore, the transmission probability \mathcal{T}_m through the m -th dot level can also be expressed in terms of the phase shift, or the density of states $\rho_{d,m}(0)$ at the Fermi level,

$$\mathcal{T}_m = \frac{4\Delta_L \Delta_R}{(\Delta_L + \Delta_R)^2} \sin^2 \delta_m, \quad (51)$$

$$\rho_{d,m}(0) \equiv -\frac{1}{\pi} \text{Im} G_m(i0^+) = \frac{\sin^2 \delta_m}{\pi \Delta}. \quad (52)$$

With this \mathcal{T}_m and $\mathcal{S}_m \equiv \mathcal{T}_m (1 - \mathcal{T}_m)$, the linear-response conductance and noise for the current flowing between the two leads, L and R , can be expressed in a Landauer form

$$\mathcal{G} = \frac{e^2}{h} \sum_{m=1}^N \mathcal{T}_m, \quad \mathcal{S} = \frac{2e^3}{h} \sum_{m=1}^N \mathcal{S}_m. \quad (53)$$

The residual interaction $\tilde{U}_{mm'}$ between the quasiparticles is another important local-Fermi-liquid parameter. It is defined in terms of the vertex correction $\Gamma_{m,m';m',m}(i\omega, i\omega'; i\omega', i\omega)$ at zero frequencies,

$$\tilde{U}_{mm'} \equiv Z_m Z_{m'} \Gamma_{m,m';m',m}(0, 0; 0, 0). \quad (54)$$

Note that $\Gamma_{mm:mm}(0, 0; 0, 0) = 0$ due to the Pauli principle. These residual interactions also become level dependent in the case where the SU(4) symmetry is broken. We introduce a dimensionless parameter $R_{mm'}$ as an analogue of the Wilson ratio in the symmetric case

$$R_{mm'} \equiv 1 + \sqrt{\tilde{\rho}_{d,m}(0)\tilde{\rho}_{d,m'}(0)} \tilde{U}_{mm'}. \quad (55)$$

Here, $\tilde{\rho}_{d,m}(0)$ is the renormalized density of states for the quasiparticles,

$$\tilde{\rho}_{d,m}(0) \equiv \frac{\rho_{d,m}(0)}{Z_m}. \quad (56)$$

The quasiparticle density of states is also one of the important parameters. For instance, contributions of the quantum-dot part on the T -linear specific heat $C_{\text{dot}} = \gamma T$ can be written as,⁴⁸

$$\gamma = \frac{\pi^2}{3} \sum_m \tilde{\rho}_{d,m}(0). \quad (57)$$

Corrections due to the residual interaction $\tilde{U}_{mm'}$ appears for higher-order correlation functions. For example, the charge susceptibility for impurity electrons can be written as $\chi_c \equiv \sum_m \chi_{c,m}$,

$$\begin{aligned} \chi_{c,m} &\equiv -\frac{\partial \langle n_{d,m} \rangle}{\partial \varepsilon_d} = -\sum_{m'} \frac{\partial \epsilon_{m'}}{\partial \varepsilon_d} \frac{\partial \langle n_{d,m} \rangle}{\partial \epsilon_{m'}} \\ &= \tilde{\rho}_{d,m}(0) \left[1 - \sum_{m'(\neq m)} \tilde{U}_{mm'} \tilde{\rho}_{d,m'}(0) \right]. \end{aligned} \quad (58)$$

Note that $\partial \epsilon_{m'}/\partial \varepsilon_d = 1$ by definition Eq. (44), the last line of Eq. (58) follows from the *Fermi-liquid relations*:

$$-\frac{\partial \langle n_{d,m} \rangle}{\partial \epsilon_{m'}} = \tilde{\rho}_{d,m}(0) \left[\delta_{mm'} - \tilde{U}_{mm'} \tilde{\rho}_{d,m'}(0) \right], \quad (59)$$

where $\tilde{U}_{mm} = 0$ by definition. These relations correspond to the Ward identities,^{48,50} described in the appendix C. The last line of Eq. (58) can also be interpreted physically such that the factor $\tilde{\rho}_{d,m}(0)$ in front represents contributions of the free renormalized quasiparticles while the bracket represents a relative dimensionless value, which is reduced from the free-quasiparticle value by the residual interactions $\tilde{U}_{mm'}$.

In order to write the magnetic susceptibilities in a similar form, we need the matrix elements of magnetization matrix $\vec{\mathcal{M}}$ with respect to one-particle eigenvector \mathbf{u}_m ,

which can be expressed in the following forms using the Feynman theorem,

$$\vec{F}_m \equiv \mathbf{u}_m^\dagger \vec{\mathcal{M}} \mathbf{u}_m = -\mathbf{u}_m^\dagger \frac{\partial \mathbf{H}_d^0}{\partial \vec{b}} \mathbf{u}_m = -\frac{\partial \epsilon_m}{\partial \vec{b}}. \quad (60)$$

The ground-state average of the magnetization $\vec{\mathcal{M}}$ can be written in terms of these matrix elements,

$$\vec{\mathcal{M}} \equiv \langle \psi_d^\dagger \vec{\mathcal{M}} \psi_d \rangle = \sum_m \vec{F}_m \langle n_{d,m} \rangle. \quad (61)$$

The magnetic susceptibility, $\chi_{\mathcal{M}}^{\mu\nu} \equiv \partial \mathcal{M}^\mu / \partial b_\nu$, can be expressed in the form,

$$\begin{aligned} \chi_{\mathcal{M}}^{\mu\nu} &= \sum_m \frac{\partial F_m^\mu}{\partial b_\nu} \langle n_{d,m} \rangle + \sum_{mm'} F_m^\mu \frac{\partial \epsilon_{m'}}{\partial b_\nu} \frac{\partial \langle n_{d,m} \rangle}{\partial \epsilon_{m'}} \\ &= \sum_m \frac{\partial F_m^\mu}{\partial b_\nu} \langle n_{d,m} \rangle + \sum_m F_m^\mu F_m^\nu \tilde{\rho}_{d,m}(0) \\ &\quad - \sum_{m \neq m'} F_m^\mu F_{m'}^\nu \tilde{\rho}_{d,m}(0) \tilde{\rho}_{d,m'}(0) \tilde{U}_{mm'}. \end{aligned} \quad (62)$$

Here, the last term in the right-hand side represents the contributions of the residual interaction, or the vertex corrections.

Specifically for $\Delta_{\text{SO}} = \Delta_{\text{KK}'} = 0$, the spin component of the magnetization becomes parallel to the field $\vec{e}_\Theta = \cos \Theta \vec{e}_z + \sin \Theta \vec{e}_x$ while the orbital component is always along the nanotube axes. Therefore, in this case Eq. (61) can be written in the form,

$$\vec{\mathcal{M}} = \mathcal{M}_{\text{orb}} \vec{e}_z + \mathcal{M}_s \vec{e}_\Theta, \quad (63)$$

$$\mathcal{M}_{\text{orb}} = g_{\text{orb}} \left[\langle n_{d,1} \rangle - \langle n_{d,4} \rangle + \langle n_{d,2} \rangle - \langle n_{d,3} \rangle \right], \quad (64)$$

$$\mathcal{M}_s = \frac{g_s}{2} \left[\langle n_{d,1} \rangle - \langle n_{d,4} \rangle - \langle n_{d,2} \rangle + \langle n_{d,3} \rangle \right]. \quad (65)$$

Here, the label $m = 1, 2, 3$ and 4 are assigned to $|K' \downarrow_{\vec{b}}\rangle$, $|K' \uparrow_{\vec{b}}\rangle$, $|K \downarrow_{\vec{b}}\rangle$ and $|K \uparrow_{\vec{b}}\rangle$, respectively, with $\uparrow_{\vec{b}}$ and $\downarrow_{\vec{b}}$ the spin defined with respect to the direction along the field \vec{b} for $\Theta < \pi/2$. The corresponding one-particle energies are given by $\epsilon_1 = \varepsilon_d - (g_{\text{orb}} \cos \Theta + g_s/2)b$, $\epsilon_2 = \varepsilon_d - (g_{\text{orb}} \cos \Theta - g_s/2)b$, $\epsilon_3 = \varepsilon_d + (g_{\text{orb}} \cos \Theta - g_s/2)b$, and $\epsilon_4 = \varepsilon_d + (g_{\text{orb}} \cos \Theta + g_s/2)b$.

V. FIELD-INDUCED CROSSOVER IN A HALF-FILLING CNT DOT

One of the most interesting experimental findings of carbon nanotube quantum dots is that the SU(4) Kondo effects for different impurity-occupation numbers $M = 1, 2$, and 3 can successively occur as the dot level ϵ_m is varied by tuning the gate voltages,¹⁶ as mentioned. We next consider a crossover from the SU(4) to SU(2) Fermi-liquid state occurring near half-filling, where two electrons are occupied in the local levels of the quantum dot.

It is a different class of the SU(4) to SU(2) crossover from those considered previously for the CNT quantum dots,^{8,9,11–13} and is inspired by recent magneto-transport experiment which observes an unexpected evolution of the Kondo plateau.¹⁹ As magnetic field increases, the Kondo plateau near half-filling reduces the height from $4e^2/h$ to $2e^2/h$ keeping the flat structure unchanged. This implies that two one-particle levels among the four still remain unlifted near the Fermi level in the magnetic field. This is possible if the magnetic field \vec{B} is applied in such a way that the spin and orbital Zeeman effects cancel each other out. In order to explain these experimental findings, we propose a model on the basis of the Anderson impurity \mathcal{H} given in Eqs. (1)–(3) with the one-particle part defined in Eqs. (41)–(43), and calculate magneto conductance and Fermi-liquid parameters using the NRG.

A. Matching of spin and orbital Zeeman splittings

We introduce a model in which the double degeneracy remains unlifted near half-filling in a finite magnetic field b , setting the parameters such that $\Delta_{\text{SO}} = \Delta_{\text{KK}'} = 0$ together with a condition

$$g_{\text{orb}} \cos \Theta = \frac{g_s}{2}, \quad g_s = 2. \quad (66)$$

This is *not* rare for CNT dots as the orbital magnetic moment can take some values around $g_{\text{orb}} \sim 10$.¹⁷ In this case, the orbital Zeeman splitting $\pm(g_{\text{orb}} \cos \Theta)b$ matches the spin Zeeman splitting $\pm(g_s/2)b$, so that the one-particle levels become

$$\epsilon_1 = \epsilon_d - 2b, \quad \epsilon_2 = \epsilon_3 = \epsilon_d, \quad \epsilon_4 = \epsilon_d + 2b. \quad (67)$$

The two levels in the middle, $m = 2$ and 3 , lost the coupling to the magnetic field as the spin and orbital Zeeman effects cancel out, and thus the energies ϵ_2 and ϵ_3 become independent of b . The other two levels, ϵ_1 and ϵ_4 , move away from ϵ_d as b increases. The total Hamiltonian \mathcal{H} has a symmetry of $U(1)_{m=1} \times SU(2)_{m=2,3} \times U(1)_{m=4}$ for finite magnetic fields. The two degenerate states, $m = 2$ and 3 , have an SU(2) symmetry while each of the other two, $m = 1$ and 4 , only has the $U(1)$ symmetry corresponding to the charge conservation of the electrons carrying the *flavor* “ m ”. This SU(2) symmetric part shows a Kondo effect which evolves from the SU(4) symmetric two-electron Kondo singlet state as magnetic field increases. Furthermore, for the one-particle levels ϵ_m given in Eq. (67), the Hamiltonian \mathcal{H} has an extended particle-hole symmetry which is accompanied by an inversion of the *flavor* “ m ”:

$$d_1^\dagger \Rightarrow h_4, \quad d_2^\dagger \Rightarrow h_3, \quad d_3^\dagger \Rightarrow h_2, \quad d_4^\dagger \Rightarrow h_1, \quad (68)$$

and $c_{\nu,\epsilon m}^\dagger \Rightarrow -f_{\nu,-\epsilon m'}$ for $(m, m') = (1, 4), (2, 3), (3, 2), (4, 1)$, where h_m and $f_{\nu,-\epsilon m'}$ are fermion operators describing the holes.

In the real CNT dot used for recent magneto-transport measurements,^{16,19} the Coulomb interaction $U \approx 6$ meV and the hybridization energy $\Delta \equiv \Delta_L + \Delta_R \approx 0.9$ meV with $\Delta_L \approx \Delta_R$ dominate the other energy scales. The valley mixing and spin-orbit interaction are smaller than these two $\Delta_{\text{KK}'} \sim \Delta_{\text{SO}} \sim 0.2$ meV. The orbital Zeeman coupling is estimated to be $g_{\text{orb}} \cos \Theta \approx 0.7$, which is still not far from the matching value 1.0. Nevertheless, in order to clarify how the deviations from the case described by Eq. (67) affect this crossover, we also examine the realistic case using ϵ_m 's determined through \mathbf{H}_d^0 with the parameters deduced from the experiment:

$$\Delta_{\text{KK}'} = \Delta_{\text{SO}} = 0.07\pi\Delta, \quad g_{\text{orb}} \cos \Theta = 0.7. \quad (69)$$

In this case, the extended particle-hole symmetry does *not* hold. Furthermore, the Hamiltonian \mathcal{H} no longer has the $SU(2)_{m=2,3}$ symmetry, and it is lowered to the $U(1)_{m=2} \times U(1)_{m=3}$ corresponding to charge conservation in each of these two channels $m = 2$ and 3 .

We have carried out NRG calculations, taking the discretization parameter to be $\Lambda = 6.0$.²¹ We have kept typically the lowest 3000 eigenstates in each NRG step using the $U(1) \times U(1) \times U(1) \times U(1)$ symmetry. The renormalized parameters have been deduced from flow of the low-energy eigenvalues near the fixed point of the NRG.^{20,21,51,52} Note that the Coulomb interaction in the above-mentioned two cases are scaled as $U = 2\pi\Delta$ with $\Delta = 0.9$ meV, and a magnetic field of order $b = 0.1\pi\Delta$ corresponds to $B = 4.9$ T in a real scale. The tunneling couplings can be well approximated by a symmetric one $\Delta_L = \Delta_R$, which simplifies the transmission probability and the current noise as $\mathcal{T}_m = \pi\Delta\rho_{d,m}(0) = \sin^2 \delta_m$ and $S_m \equiv \mathcal{T}_m(1 - \mathcal{T}_m) = (\sin^2 2\delta_m)/4$, respectively.

B. $U(1)_{m=1} \times SU(2)_{m=2,3} \times U(1)_{m=4}$ symmetric case

The conductance \mathcal{G} obtained for energy levels ϵ_m given in Eq. (67) is plotted vs ϵ_d in the upper panel of Fig. 2 for several values of b . The lower panel shows $\sin^2 \delta_m$ and $\langle n_m \rangle$ for $m = 1, 2, 3, 4$ at $b/(\pi\Delta) = 0.2$. We can see that the conductance has a broad peak near half-filling $\epsilon_d/U \simeq -1.5$. The system has the SU(4) symmetry at zero field $b = 0$, and the conductance peak reaches the unitary-limit value $4e^2/h$. Because the interaction $U/(\pi\Delta) = 2.0$ is still not very large, the conductance peak is not completely flat and the shoulders near 1/4 and 3/4 fillings are less pronounced. Such a flat structure will become clearer if the Coulomb interaction U is much larger. Nevertheless, other Fermi-liquid parameters are already renormalized significantly,^{34,35} as we will describe later.

As magnetic field b increases, the broad conductance peak decreases and in the limit of $b \rightarrow \infty$ it approaches the SU(2) unitary-limit value $2e^2/h$, keeping the typical flat form of the Kondo plateau. This is caused by the doubly degenerate levels $m = 2$ and 3 remaining at

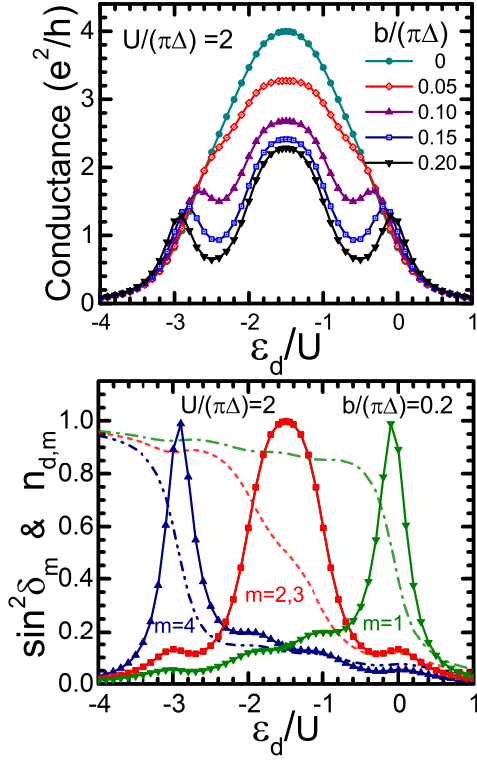


FIG. 2. (Color online) NRG results are plotted vs ϵ_d for ϵ_m given in Eq. (67) and $U/(\pi\Delta) = 2.0$. Upper panel: conductance at magnetic fields of $b/(\pi\Delta) = 0, 0.05, 0.1, 0.15,$ and 0.2 . Lower panel: $\sin^2 \delta_m$ (solid line) and $\langle n_{d,m} \rangle$ (dashed line) at $b/(\pi\Delta) = 0.2$ which corresponds to a real field of $B = 9.8$ T for $\Delta = 0.9$ meV.¹⁶

the Fermi level, and is consistent with the behavior observed in the recent measurements.¹⁹ The contributions of the other two levels, $m = 1$ and 4 , on the conductance are separately seen for large fields $b/(\pi\Delta) \gtrsim 0.1$ as the two additional sub peaks at $\epsilon_d/U \approx 0.0$ and -3.0 with the height close to e^2/h . We can also see in the lower panel of Fig. 2, which shows the results at $b/(\pi\Delta) = 0.2$, that two of the channels $m = 2$ and 3 contribute to the SU(2) Kondo plateau near half-filling while the other two contribute to the side peaks. Furthermore, $\sin^2 \delta_m$ has a long tail in the off-resonance region with a weak step-structure that is caused by the inter-channel correlations. The steps emerge as the resonance peaks cross the Fermi level. The phase shift δ_m varies from 0 to π for $m = 1$ and 4 at the crossing point as a single electron enters into the impurity level. The Kondo half-step $\delta_m = \pi/2$ emerges near half-filling $\epsilon_d/U \simeq -1.5$ for the levels $m = 2$ and 3 in the middle, and this half-step will be more pronounced if U is much larger.

The Kondo effect which is caused by the doubly degenerate states, $m = 2$ and 3 , is most enhanced at half-filling $\epsilon_d/U = -3/2$. We next investigate the magnetic field dependence of the Kondo correlations in more detail at half-filling. Figure 3 shows $\langle n_m \rangle$, $\sin^2 \delta_m$, and

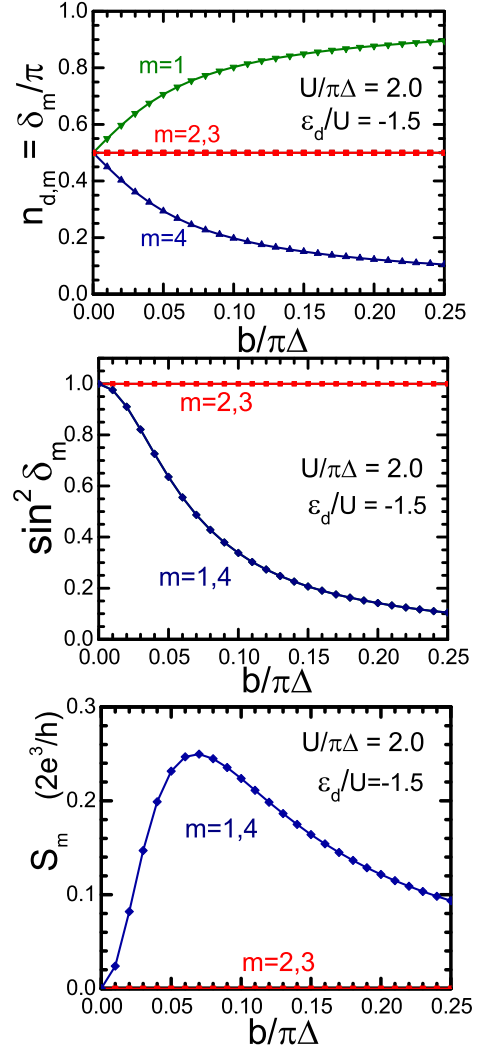


FIG. 3. (Color online) $\langle n_{d,m} \rangle = \delta_m/\pi$, $\sin^2 \delta_m$, and current noise S_m are plotted vs b at half-filling $\epsilon_d/U = -1.5$ and $U/(\pi\Delta) = 2.0$ for ϵ_m given in Eq. (67).

the current noise S_m as a function of b . Even at finite magnetic fields b , the average occupation number of the twofold degenerate states, $m = 2$ and 3 , is unchanged $\langle n_2 \rangle = \langle n_3 \rangle = 1/2$. This is caused by the matching of spin and orbital Zeeman splittings described by Eq. (66). As the phase shifts are locked at $\delta_2 = \delta_3 = \pi/2$, these two channels give a unitary-limit contribution $2e^2/h$ to the total conductance and do not induce a current noise $S_2 = S_3 = 0$. The transmission probability of the other two levels ($\sin^2 \delta_1 = \sin^2 \delta_4$) decreases as b increases and finally vanish in the limit of $b \rightarrow \infty$. Correspondingly, the current noise for these states ($S_1 = S_4$) has a maximum at $b/(\pi\Delta) \approx 0.07$ where the transmission probability becomes $\mathcal{T}_1 = \mathcal{T}_4 = 0.5$, namely at the filling of $\langle n_{d,4} \rangle = 1/4$ and $\langle n_{d,1} \rangle = 3/4$. Owing to the matching condition Eq. (66), the magnetization $\vec{\mathcal{M}}$ given in Eqs. (63)–(65) can be expressed in the form $\mathcal{M}_{\text{orb}} = g_{\text{orb}} \mathcal{M}_{14}$

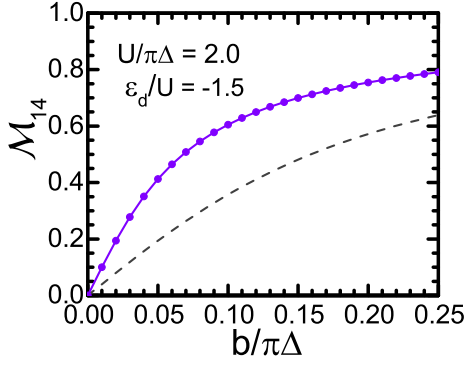


FIG. 4. (Color online) Magnetization \mathcal{M}_{14} defined in Eq. (70) is plotted vs b at half-filling $\epsilon_d/U = -1.5$ and $U/(\pi\Delta) = 2.0$ for ϵ_m given in Eq. (67). The dashed line shows the noninteracting results obtained for $U = \epsilon_d = 0$.

and $\mathcal{M}_s = \frac{g_s}{2}\mathcal{M}_{14}$ with

$$\mathcal{M}_{14} \equiv \langle n_{d,1} \rangle - \langle n_{d,4} \rangle. \quad (70)$$

Both the spin and orbital components of the magnetization are determined by the phase shifts of the first and fourth levels: $\delta_1 = \pi(1 + \mathcal{M}_{14})/2$ and $\delta_4 = \pi(1 - \mathcal{M}_{14})/2$. We see in Fig. 4 that \mathcal{M}_{14} is significantly enhanced by the Coulomb interaction U , and it approaches to the saturation value 1 for large fields. In the limit of $b \rightarrow \infty$, both the charge and magnetic fluctuations caused by these two levels are suppressed as the occupation numbers tend to be full $\langle n_1 \rangle \rightarrow 1$ and empty $\langle n_4 \rangle \rightarrow 0$.

Thus, in the limit of large magnetic field $b \rightarrow \infty$, most of the components of the Coulomb interaction defined in Eq. (1) can be treated with the mean-field theory, except for the one between the twofold degenerate levels, $m = 2$ and $m' = 3$.⁵³ Thus, the dot part of the Hamiltonian can be simplified in the form,

$$\begin{aligned} \mathcal{H}_d \xrightarrow{b \rightarrow \infty} & U \left[n_2 n_3 - \frac{1}{2} (n_2 + n_3) \right] \\ & + \left(2b + \frac{U}{2} \right) (n_4 - n_1) + \text{const.} \end{aligned} \quad (71)$$

This shows that the degenerate levels remaining at the Fermi level, $m = 2$ and 3, can be described by the particle-hole symmetric SU(2) Anderson model. The other two levels, $m = 1$ and 4, are frozen and can be separated. As discussed in Sec. II and III, the ground-state wavefunction for the two-site case gives an insight into the Fermi-liquid fixed point. For large fields and $U \gg \Delta$, dominant components of the ground state are given by

$$|\Psi\rangle_{2\text{site}} \propto \left(a_2^\dagger b_2^\dagger + a_3^\dagger b_3^\dagger \right) a_1^\dagger b_1^\dagger |\tilde{0}\rangle + \dots \quad (72)$$

$$= \left(a_2^\dagger a_3^\dagger - a_3^\dagger a_2^\dagger \right) a_1^\dagger a_4^\dagger |0\rangle + \dots \quad (73)$$

where $|\tilde{0}\rangle = a_1^\dagger a_2^\dagger a_3^\dagger a_4^\dagger |0\rangle$ and b_m^\dagger is the creation operator for the conduction hole defined in Eq. (20). This wave-

$$|\Psi\rangle_{2\text{site}} \simeq \begin{array}{c} d^\dagger \quad b^\dagger \\ 4 \quad \color{red}\blacksquare \quad \color{white}\square \\ 3 \quad \color{white}\square \quad \color{white}\square \\ 2 \quad \bullet \quad \circ \\ 1 \quad \color{cyan}\bullet \quad \circ \end{array} + \begin{array}{c} d^\dagger \quad b^\dagger \\ 4 \quad \color{red}\blacksquare \quad \color{white}\square \\ 3 \quad \bullet \quad \circ \\ 2 \quad \color{white}\square \quad \color{white}\square \\ 1 \quad \color{cyan}\bullet \quad \circ \end{array} + \dots$$

FIG. 5. (Color online) Schematic picture of the ground-state wave function near the CNT dot for large fields and $U \gg \Delta$. Each row represents one of the levels $m = 1, 2, 3, 4$. The first (d^\dagger) and second (b^\dagger) columns represent orbitals in the impurity and the adjacent conduction site, respectively, with (\bullet) the impurity-electrons and (\circ) the conduction-holes. The explicit expression of the wavefunction is given in Eq. (72). The impurity level of $m = 1$ (4), which is illustrated as a light blue (red) box, sits deep inside (far above) the Fermi level, and thus corrections of order v^2/b determine the distribution of the conduction-hole next to these colored boxes.

function is also illustrated in Fig. 5. The singlet pair state is constructed by the electrons at $m = 2$ and 3, which can evolve to the Fermi-liquid state, for instance, through the successive NRG steps that take into account the low-energy conduction-electron degrees of freedom. The particle-hole pair is localized at the bottom ($m = 1$) and is absent at the top ($m = 4$). The corrections of order v^2/b due to virtual tunneling processes determine the distribution of the conduction electrons at $m = 1$ and $m = 4$ shown in Fig. 5.

How each resonance level shifts as magnetic field increases can be tracked through $\tilde{\epsilon}_m$ shown in the top panel of Fig. 6. As already deduced from other data, the resonance peak for the doubly degenerate states stays just on the Fermi level as $\tilde{\epsilon}_2 = \tilde{\epsilon}_3 = 0$. The peaks for the other two, $\tilde{\epsilon}_1$ and $\tilde{\epsilon}_4$, move far away from the Fermi level as b increases. The slope of $\tilde{\epsilon}_1$ and $\tilde{\epsilon}_4$ against b become steeper than those for the noninteracting case. This difference causes the enhancement of the magnetization \mathcal{M}_{14} described in Fig. 4. For large b , these two levels asymptotically approach $\pm(2b + \frac{U}{2})$, given in Eq. (71).

The continuous evolution from the Fermi-liquid state with the SU(4) symmetry to the one with the SU(2) appears more sensitively in the field-dependence of the renormalization factor Z_m and the residual interaction $\tilde{U}_{mm'}$ shown in the middle and bottom panels of Fig. 6. Note that $Z_2 = Z_3$ and $Z_1 = Z_4$ because of the symmetry described in Eq. (68), and there are three independent components for $R_{mm'}$: R_{23} , R_{14} , and $R_{12} = R_{13} = R_{24} = R_{34}$. Especially, the coefficients Z_2 and R_{23} for the doubly degenerate states at the Fermi level continuously evolve from the SU(4) value to the SU(2) value as b varies from 0 to ∞ . At zero field, these coefficients take the SU(4) values: $Z_{\text{SU4}} = 0.52$ and $R_{\text{SU4}} - 1 = 0.31$ for $U/(\pi\Delta) = 2.0$. In the opposite limit $b \rightarrow \infty$, these two parameters approach those for the SU(2) Anderson model: $Z_2 \rightarrow 0.24$ and $R_{23} - 1 \rightarrow 0.96$ for the same U . The parameters for the other two levels approach the noninteracting value in the limit of large magnetic

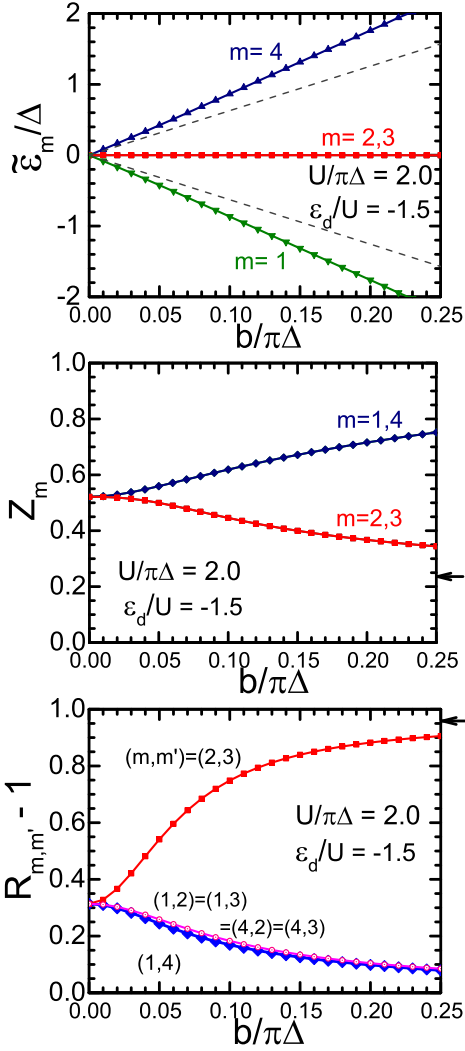


FIG. 6. (Color online) Renormalized parameters $\tilde{\epsilon}_m$, Z_m and $R_{mm'} - 1$ plotted vs b at half-filling $\epsilon_d/U = -1.5$ and $U/(\pi\Delta) = 2.0$ for ϵ_m given in Eq. (67). The dashed line in the top panel shows the noninteracting level position for $U = 0$. Arrows in the middle and bottom panels indicate the corresponding values in the $SU(2)$ limit.

field $b \rightarrow \infty$: namely $Z_1 \rightarrow 1$, $R_{12} \rightarrow 1$, and $R_{14} \rightarrow 1$. Note that R_{12} is slightly larger than R_{14} for finite b as the energy separation $\tilde{\epsilon}_2 - \tilde{\epsilon}_1$ is the half of $\tilde{\epsilon}_4 - \tilde{\epsilon}_1$. All these results shown in the subsection indicate that quantum fluctuations and many-body renormalization effects are enhanced as b increases because the number of active channels decreases as the two levels, $m = 1$ and 4 , among the four are frozen.

Figure 7 shows the charge susceptibility $\chi_{c,m}$, which is obtained using these results of the Wilson ratio with Eqs. (55) and (58). The component for $m = 1$ and 4 ($\chi_{c,1} = \chi_{c,4}$) decreases as b increases because these two levels are frozen for large magnetic fields. In the present case, Eq. (58) can be rewritten in the following form for

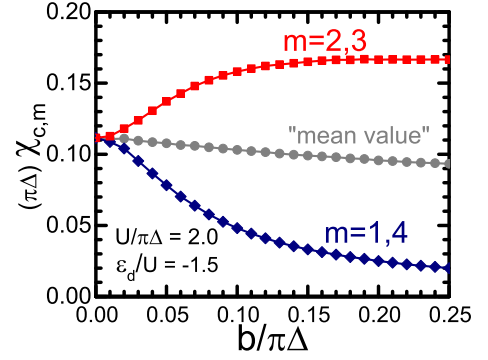


FIG. 7. (Color online) Charge susceptibility $\chi_{c,m}$ plotted vs b for $m = 1, 2, 3, 4$ at half-filling, $\epsilon_d/U = -1.5$ and $U/(\pi\Delta) = 2.0$ for ϵ_m given in Eq. (67). The line in the middle denotes a normalized total susceptibility $(\pi\Delta/4) \sum_m \chi_{c,m}$.

the component for $m = 2$ and 3 ($\chi_{c,2} = \chi_{c,3}$),

$$\pi\Delta \chi_{c,2} = \frac{1}{Z_2} \left[1 - (R_{23} - 1) - 2(R_{12} - 1) \sqrt{\frac{Z_2 \sin^2 \delta_1}{Z_1 \sin^2 \delta_2}} \right]. \quad (74)$$

Here, the prefactor $1/Z_2$ represents an enhancement of the quasiparticle density of states for $m = 2$ (or 3) whereas the bracket represents magnitude of the susceptibility relative to the one for free renormalized quasiparticles. The $SU(2)_{m=2,3}$ part of $\chi_{c,2}$ becomes larger than that for the $SU(4)$ symmetric case because the enhancement due to the quasiparticle density of states for $m = 2$ and 3 dominates the reduction due to the residual interactions. The total impurity susceptibility $\chi_c = \sum_m \chi_{c,m}$ is suppressed as magnetic field increases.

C. Perturbations that break the $SU(2)_{m=2,3}$

We next take into account the perturbations that break the $SU(2)_{m=2,3}$ symmetry and lift the double degeneracy of the one-particle levels at the Fermi level, discussed in the above. Typical parameter values for such perturbations in a real CNT dot are given in Eq. (69). The valley mixing $\Delta_{KK'}$ and the spin-orbit interaction Δ_{SO} open the gap in the four one-particle levels. For $g_{\text{orb}} \cos \Theta \neq g_s/2$, the matching of the spin and orbital Zeeman splittings becomes no longer perfect. Furthermore, an extended particle-hole symmetry such as Eq. (68) does not hold at finite parallel fields $b_{\parallel} \neq 0$ in the case where $\Delta_{SO} \neq 0$.

At zero-field $b = 0$, the eigenvalues of \mathbf{H}_d^0 can be explicitly written as^{13,14}

$$\epsilon_d \pm \frac{1}{2} \sqrt{\Delta_{KK'}^2 + \Delta_{SO}^2}. \quad (75)$$

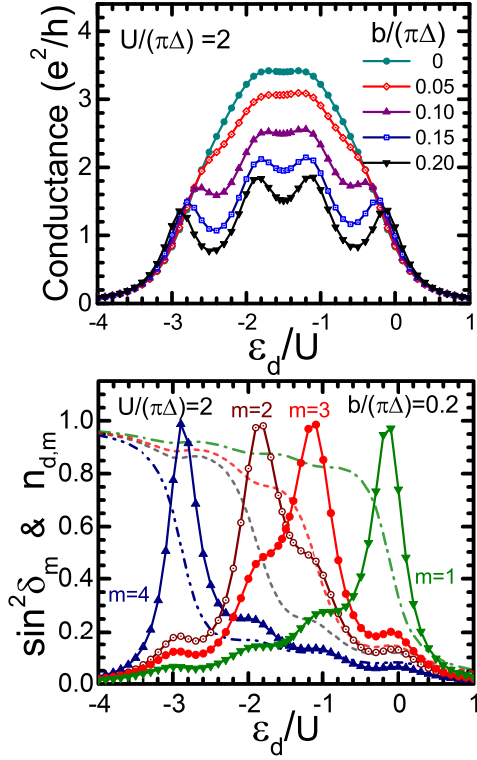


FIG. 8. (Color online) NRG results are plotted vs ϵ_d for ϵ_m deduced from Eq. (69) and $U/(\pi\Delta) = 2.0$, Upper panel: conductance at magnetic fields of $b/(\pi\Delta) = 0, 0.05, 0.1, 0.15,$ and 0.2 . Lower panel: $\sin^2 \delta_m$ (solid line) and $\langle n_{d,m} \rangle$ (dashed line) at $b/(\pi\Delta) = 0.2$, which corresponds to a real field of $B = 9.8$ T for $\Delta = 0.9$ meV.¹⁶

Thus, $\sqrt{\Delta_{\text{KK}'}^2 + \Delta_{\text{SO}}^2}$ is the energy gap between the two different groups of the one-particle levels. The eigenvectors are doubly degenerate, which is caused by an $\text{SU}(2)$ symmetry defined with respect to the $\bar{\sigma} = (\uparrow, \downarrow)$ component of the operator $g_{\bar{\tau}, \bar{\sigma}}$:

$$\begin{pmatrix} g_{+, \uparrow} \\ g_{-, \uparrow} \end{pmatrix} \equiv \begin{pmatrix} \psi_{\text{K}\uparrow} \\ \psi_{\text{K}'\uparrow} \end{pmatrix}, \quad \begin{pmatrix} g_{+, \downarrow} \\ g_{-, \downarrow} \end{pmatrix} \equiv \begin{pmatrix} \psi_{\text{K}'\downarrow} \\ \psi_{\text{K}\downarrow} \end{pmatrix}. \quad (76)$$

In addition, just at $b = 0$, an extended particle-hole symmetry holds as a result of an invariance with respect to the transformation,

$$g_{+, \bar{\sigma}}^\dagger \Rightarrow -h_{-, \bar{\sigma}}, \quad g_{-, \bar{\sigma}}^\dagger \Rightarrow h_{+, \bar{\sigma}}, \quad (77)$$

with the corresponding transforms similar to those shown in Eq. (68) for conduction electrons.

Figure 8 shows the NRG results obtained for the parameter set given in Eq. (69) as a function of ϵ_d . We have chosen the same values for the Coulomb interaction U and hybridization energy scale Δ with $\Delta_L = \Delta_R$ as those for the $\text{SU}(2)_{m=2,3}$ symmetric case. In the upper panel, the linear conductance \mathcal{G} is plotted for several values of the magnetic field b . We see that a flat plateau emerges for $-2.0 \lesssim \epsilon_d/U \lesssim -1.0$ at zero field

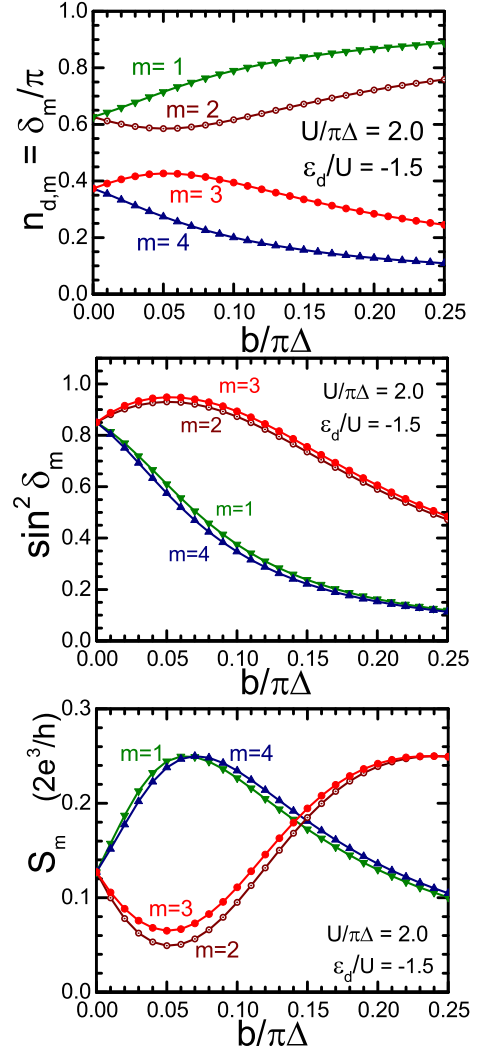


FIG. 9. (Color online) $\langle n_{d,m} \rangle = \delta_m/\pi$, $\sin^2 \delta_m$, and current noise \mathcal{S}_m are plotted vs b for $\epsilon_d = -1.5U$ and $U/(\pi\Delta) = 2.0$, and ϵ_m deduced from Eq. (69).

although the height $\mathcal{G} \approx 3.4 e^2/h$ is smaller than the unitary limit value. This can be compared to the results shown in Fig. 2. The flat structure which is consistent with the recent measurements¹⁹ is still preserved for small fields $b/(\pi\Delta) \lesssim 0.1$, namely up to $B \approx 5.0$ T in real scale of magnetic field. For larger fields $b/(\pi\Delta) \gtrsim 0.1$, the plateau deforms into two separate peaks, and also there emerge the other two outer sub-peaks. We can also see in the lower panel of Fig. 8 how the four conductance peaks are decomposed into the contributions of each conducting channel m at $b/(\pi\Delta) = 0.2$. The separation between the two peaks in the middle and their width determine a magnitude of the field, at which the plateau collapses. Such a field depends significantly on the Fermi-liquid corrections.⁵⁴ The peak structures in the lower panel also represent the density of states at the Fermi level, defined in Eq. (52). The density of

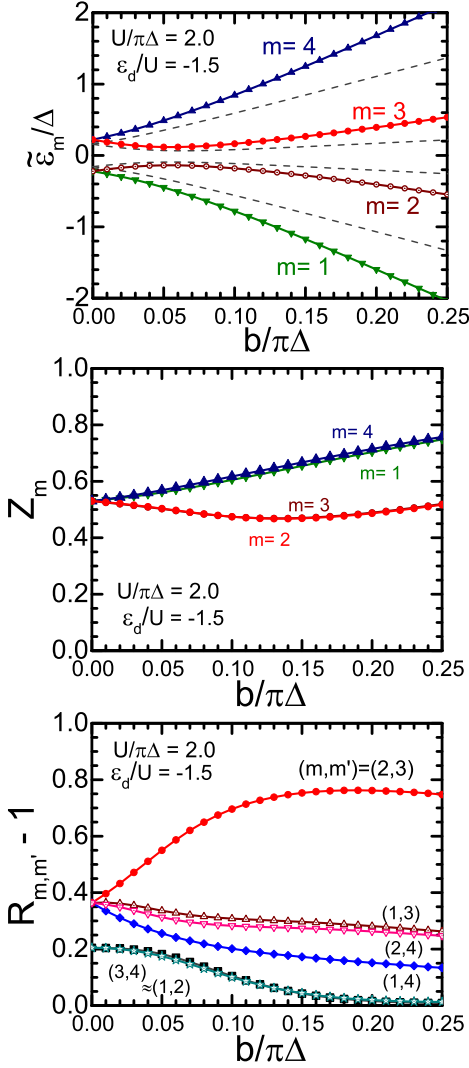


FIG. 10. (Color online) Resonance position $\tilde{\epsilon}_m$, Z_m and $R_{mm'} - 1$ plotted vs b for $\epsilon_d = -1.5U$ and $U/(\pi\Delta) = 2.0$, and ϵ_m deduced from Eq. (69). The dashed line in the top panel shows the noninteracting level position for $U = 0$.

states, $\rho_{d,m}(0) = \sin^2 \delta_m / (\pi\Delta)$, has a long tail in the off-resonance region with some steps, at which a resonance peak crosses the Fermi level and the occupation number $\langle n_{d,m} \rangle$ shows an abrupt change. Note that these results are *not* fully symmetric with respect to the point $\epsilon_d = -1.5U$, except for $b = 0$, as the particle-hole symmetry defined in Eq. (77) does not hold for $b \neq 0$.

In Fig. 9, the NRG results that have been deduced from the phase shift δ_m are plotted as a function of the magnetic field b , for $\epsilon_d = -1.5U$. These results can be compared with those shown in Fig. 3 for the $SU(2)_{m=2,3}$ symmetry case. We see in the top panel that the phase shift for $m = 2$ and that for $m = 3$ are *not* locked at $\pi/2$ in the preset case. This is because that the gap due to the valley mixing and spin-orbit interaction lifts the degeneracy and the cancellation between the spin and orbital Zeeman effects does *not* occur. Nevertheless, these

phase shifts, δ_2 and δ_3 , take the values which are not far from $\pi/2$ for $b/(\pi\Delta) \lesssim 0.1$, and these two approach closest to each other at $b/(\pi\Delta) \approx 0.05$. Correspondingly, the transmission probabilities through these two levels take the values around $\sin^2 \delta_2 \simeq \sin^2 \delta_3 \approx 0.9$. The current noise becomes finite in the presence of the perturbations but it is still not large $S_2 \simeq S_3 \approx 0.3$ for $b/(\pi\Delta) \lesssim 0.1$. The behavior of the other two levels, $m = 1$ and $m = 4$, are similar to those in the $SU(2)_{m=2,3}$ symmetry case shown in Fig. 3, except for the region near zero field $b/(\pi\Delta) \approx 0.0$, where the energy gap due to $\Delta_{KK'}$ and Δ_{SO} dominate the spin and orbital Zeeman splittings for $m = 1$ and $m = 4$.

Figure 10 shows the results of the renormalized local-Fermi-liquid parameters, obtained for the same parameter set. At zero magnetic field, all the wavefunction renormalization factors, namely Z_m for $m = 1, 2, 3, 4$, become identical. Furthermore, the Wilson ratio $R_{mm'}$, or the residual interaction $\tilde{U}_{mm'}$, has two independent components at $b = 0$: $R_{12} = R_{34}$ between two different levels with the same energy, and $R_{23} = R_{13} = R_{24} = R_{14}$ between two levels separated by the gap. This is caused by the $SU(2)$ and extended particle-hole symmetries, described in Eqs. (76) and (77). We see in the middle and bottom panels that the renormalization factors Z_2 and Z_3 , and residual interactions $R_{23} - 1$, for the two levels in the middle $m = 2$ and 3 , show a clear crossover behavior which is quite similar to those for the $SU(2)_{m=2,3}$ symmetric case shown in Fig. 6. Namely, at $b/(\pi\Delta) \lesssim 0.1$, Z_2 and Z_3 decrease and simultaneously $R_{23} - 1$ increases as the other two outside levels $\tilde{\epsilon}_1$ and $\tilde{\epsilon}_4$ move away from the Fermi level. It represents that electron correlations are enhanced as the fluctuations due to the levels $m = 1$ and 4 are suppressed. Note that the results for Z_2 and those for Z_3 almost overlap each other in the middle panel.

The top panel of Fig. 10 shows the position of renormalized resonance $\tilde{\epsilon}_m$ (solid line) and that of the bare one ϵ_m (dashed line). For small fields, the two levels $\tilde{\epsilon}_2$ and $\tilde{\epsilon}_3$ near the Fermi level approach closer to each other until they reach the extreme points at $b/(\pi\Delta) \approx 0.05$. Then, these two levels separate again for large fields. At the extreme point, the peak separation becomes $\tilde{\epsilon}_3 - \tilde{\epsilon}_2 \approx 0.25\Delta$. This is still smaller than the renormalized resonance width $\tilde{\Delta}_m \equiv Z_m \Delta \sim T_K$ because $Z_2 \simeq Z_3 \approx 0.5$. The situation, $\tilde{\epsilon}_3 - \tilde{\epsilon}_2 \lesssim T_K$, does not change for $b \lesssim 0.1\pi\Delta$, namely up to $B \approx 5.0$ T. Thus, although two resonance peaks at $\tilde{\epsilon}_2$ and $\tilde{\epsilon}_3$ are separated in the realistic case of Eq. (69), the superposition of these two form a single broad peak at the Fermi level for $b/(\pi\Delta) \lesssim 0.1$ and determines the low-energy behavior.

We can also see in the middle panel that Z_2 and Z_3 take a minimum at $b/(\pi\Delta) \approx 0.13$, which is larger than the extreme points of $\tilde{\epsilon}_2$ and $\tilde{\epsilon}_3$, and also than those of the occupation number $\langle n_{d,2} \rangle$ and $\langle n_{d,3} \rangle$. This is caused by the fact that evolution of Z_2 and Z_3 also depends sensitively on the the occupation numbers, $\langle n_{d,1} \rangle$ and $\langle n_{d,4} \rangle$, of the other two levels $m = 1$ and 4 . We see in the

top panel of Fig. 9 that $\langle n_{d,1} \rangle$ and $\langle n_{d,4} \rangle$ still show a linear dependence on b at the extreme point of $\langle n_{d,2} \rangle$ and $\langle n_{d,3} \rangle$, near $b/(\pi\Delta) \approx 0.05$. Around this point of magnetic field b , the renormalization factors Z_2 and Z_3 still decrease as the variations of $\langle n_{d,1} \rangle$ and $\langle n_{d,4} \rangle$ dominate those of $\langle n_{d,2} \rangle$ and $\langle n_{d,3} \rangle$.

VI. SUMMARY

We have shown that the $SU(N)$ Fermi-liquid fixed point that Nozières and Blandin suggested for general impurity-electrons filling M can be interpreted as a Perron-Frobenius eigenvector for the composite pairs, each of which consists of one impurity-electron and one conduction-hole carrying the same *flavor* “ m ”. It is equivalent to the *totally antisymmetric representation* in the $SU(N)$ symmetric case. The description in terms of the bosonic Perron-Frobenius vector does *not* require the $SU(N)$ symmetry, and this unique nodeless eigenvector can evolve in a certain region of the Hilbert space keeping its components *positive definite*. This is one significant advantage of the hard-core boson interpretation, and it also clarifies that the *hole picture*, which is introduced only for conduction electrons, can naturally describe evolutions of the Fermi-liquid fixed point for $M \leq N/2$. As an example, we have considered the ground-state wavefunction of an anisotropic Coqblin-Schrieffer model with M impurity-electrons in the limit of strong exchange couplings.

One of the most interesting features of carbon nanotube quantum dot is that various kinds of Kondo effects occur in a tunable-parameter space. We have shown that the field-induced crossover from the $SU(4)$ to $SU(2)$ Fermi-liquid behavior, which has been observed in recent experiments at two impurity-electrons filling, can be explained as a result of a matching of the spin and orbital Zeeman splittings. It yields an emergent $SU(2)$ symmetry, which induces the Kondo effect that is not suppressed by magnetic fields. Such a matching is expected to be *not* rare for nanotube dots, at least approximately, as the orbital magnetic moment g_{orb} can take a larger value than the spin magnetic moment $g_s/2$. NRG calculations have been carried out *i)* for the case with this emergent $SU(2)$ symmetry, and *ii)* for the other case where realistic perturbations that break this symmetry are taken into account. The results for the linear-conductance show the behavior that is consistent with the measurements, which observe that the height of the Kondo plateau decreases as the field increases keeping the flat structure. This behavior can also be seen for a realistic parameter set at magnetic fields of $B \lesssim 5.0$ T where the level splitting, which is caused by the valley mixing, the spin-orbit coupling, and mismatching of the spin and orbital Zeeman effects, becomes smaller than the Kondo energy scale T_K . Furthermore, the NRG results of the local-Fermi-liquid parameters for quasiparticles show that quantum fluctuations are enhanced as the number of active one-particle

levels gradually decreases from 4 to 2. These results will be compared with the experiments elsewhere.¹⁹

ACKNOWLEDGMENTS

This work was supported by JSPS KAKENHI Grant Numbers JP26220711, JP26400319, JP16K17723, and JP15K17680.

Appendix A: $SU(N)$ Kondo model for general M

1. Hubbard operators & $SU(N)$ generators

The Coqblin-Schrieffer model can be written in the form of the $SU(N)$ Kondo model, using a relation between the Hubbard operators and the $SU(N)$ generators. The first term of the Coqblin-Schrieffer Hamiltonian, given in Eq. (12) can be expressed in the form

$$\begin{aligned} \sum_{mm'} a_m^\dagger a_{m'} d_m^\dagger d_m &= \sum_{mm'} \left(\mathbf{a}^\dagger \mathbf{X}^{mm'} \mathbf{a} \right) \left(\mathbf{d}^\dagger \mathbf{X}^{m'm} \mathbf{d} \right) \\ &= \frac{1}{N} \left(\mathbf{a}^\dagger \mathbf{1} \mathbf{a} \right) \left(\mathbf{d}^\dagger \mathbf{1} \mathbf{d} \right) + 2 \left(\mathbf{a}^\dagger \mathbf{T}^\mu \mathbf{a} \right) \left(\mathbf{d}^\dagger \mathbf{T}^\mu \mathbf{d} \right). \end{aligned} \quad (\text{A1})$$

Here, $\mathbf{X}^{mm'}$ is an $N \times N$ matrix version of the Hubbard operator corresponding to $|m\rangle\langle m'|$, namely it has a single non-zero element with the value 1 at (m, m') and all the other elements are zero. The second line of Eq. (A1) follows from a matrix identity which corresponds to the completeness relation,⁴²

$$\sum_{m=1}^N \sum_{m'=1}^N \mathbf{X}^{mm'} \otimes \mathbf{X}^{m'm} = \frac{1}{N} \mathbf{1} \otimes \mathbf{1} + 2 \mathbf{T}^\mu \otimes \mathbf{T}^\mu. \quad (\text{A2})$$

It can be proved using the explicit expressions of \mathbf{T}^μ ,

$$\mathbf{T}^{(k+1)^2-1} \equiv \frac{1}{\sqrt{2k(k+1)}} \left(\sum_{m=1}^k \mathbf{X}^{mm} - k \mathbf{X}^{k+1,k+1} \right), \quad (\text{A3})$$

$$\mathbf{T}^{k^2-2+2j} \equiv \frac{\mathbf{X}^{j,k+1} + \mathbf{X}^{k+1,j}}{2}, \quad (\text{A4})$$

$$\mathbf{T}^{k^2-1+2j} \equiv \frac{\mathbf{X}^{j,k+1} - \mathbf{X}^{k+1,j}}{2i}, \quad (\text{A5})$$

where $j = 1, 2, \dots, k$, and $k = 1, 2, \dots, N-1$. The assignment of $\mu = 1, 2, \dots, N^2-1$ for \mathbf{T}^μ , follows a conventional way of labeling the Gell-Mann matrices $\boldsymbol{\lambda}^\mu \equiv \mathbf{T}^\mu/2$ of the $SU(N)$. These matrices have the properties: $\text{Tr}[\mathbf{T}^\mu] = 0$, and

$$\text{Tr}[\mathbf{T}^\mu \mathbf{T}^\nu] = \frac{1}{2} \delta^{\mu\nu}, \quad \mathbf{T}^\mu \mathbf{T}^\mu = \frac{N^2-1}{2N} \mathbf{1}. \quad (\text{A6})$$

Here, $\mathbf{1}$ is the $N \times N$ unit matrix.

2. Fock space for M impurity-electrons

There are $\binom{N}{M}$ configurations to distribute M electrons into N impurity levels,

$$|\{\alpha\}\rangle_M \equiv d_{\alpha_1}^\dagger d_{\alpha_2}^\dagger \cdots d_{\alpha_M}^\dagger |0\rangle. \quad (\text{A7})$$

Here, $\{\alpha\} = \{\alpha_1, \alpha_2, \dots, \alpha_M\}$ represents a set of M occupied impurity levels. This state can be regarded as an *antisymmetric representation* of the $SU(N)$. With this basis set, the operator $(\mathbf{d}^\dagger \mathbf{T}^\mu \mathbf{d})$ can be written in a matrix form,

$$\left\{ \mathcal{S}_{r_M}^\mu \right\}_{\alpha' \alpha} = {}_M \langle \{\alpha'\} | \mathbf{d}^\dagger \mathbf{T}^\mu \mathbf{d} | \{\alpha\} \rangle_M. \quad (\text{A8})$$

The Casimir operator for this representation is given by

$$\mathcal{S}_{r_M}^\mu \mathcal{S}_{r_M}^\mu = C_2(r_M) \mathcal{I}_{r_M}, \quad (\text{A9})$$

$$C_2(r_M) \equiv \frac{M(N-M)(N+1)}{2N}. \quad (\text{A10})$$

Here, \mathcal{I}_{r_M} is the $\binom{N}{M}$ dimensional unit matrix.

3. Poor man's scaling for M impurity-electrons

The one-loop scaling equation for M impurity-electrons can be obtained in a symmetric way, using the exchange interaction given in Eq. (18). Following the standard prescription,^{1,36} we introduce $\tilde{D} = D - \delta D$ for the bonding components of conduction electrons $c_{\epsilon m} \equiv \sum_{\nu=L,R} v_\nu c_{\nu, \epsilon m} / v$, and obtain the order J_K^2 corrections,

$$\begin{aligned} \delta \mathcal{H}_K^{(M)} &= J_K^2 \rho_c \int_{-D}^D d\epsilon d\epsilon' \left[\int_{\tilde{D}}^D d\xi d\xi' c_{\epsilon'}^\dagger \mathbf{T}^\mu c_\xi \mathcal{S}_{r_M}^\mu \frac{\rho_c}{\omega - D + \epsilon} c_{\xi'}^\dagger \mathbf{T}^\nu c_\epsilon \mathcal{S}_{r_M}^\nu \right. \\ &\quad \left. + \int_{-D}^{-\tilde{D}} d\xi d\xi' c_{\xi'}^\dagger \mathbf{T}^\nu c_\epsilon \mathcal{S}_{r_M}^\nu \frac{\rho_c}{\omega - D - \epsilon'} c_{\epsilon'}^\dagger \mathbf{T}^\mu c_\xi \mathcal{S}_{r_M}^\mu \right] \\ &\simeq J_K^2 \frac{\rho_c \delta D}{\omega - D} \mathbf{a}^\dagger \mathbf{T}^\mu \mathbf{T}^\nu \mathbf{a} \left(\mathcal{S}_{r_M}^\mu \mathcal{S}_{r_M}^\nu - \mathcal{S}_{r_M}^\nu \mathcal{S}_{r_M}^\mu \right) \\ &= J_K^2 \frac{\rho_c \delta D}{\omega - D} \left(-\frac{1}{2} \right) f^{\mu\nu\lambda} f^{\mu\nu\lambda'} \mathbf{a}^\dagger \mathbf{T}^{\lambda'} \mathbf{a} \mathcal{S}_{r_M}^\lambda \\ &= J_K^2 \frac{\rho_c \delta D}{\omega - D} \left(-\frac{N}{2} \right) \mathbf{a}^\dagger \mathbf{T}^\lambda \mathbf{a} \mathcal{S}_{r_M}^\lambda. \quad (\text{A11}) \end{aligned}$$

Here, the factor N emerges from $f^{\mu\nu\lambda} f^{\mu\nu\lambda'} = N \delta^{\lambda\lambda'}$.⁴³ From Eq. (A11) the scaling equation, which obviously agrees with the results of Nozières and Blandin given in Eq. (14) of Ref. 22, follows

$$-\frac{d}{d\tilde{D}} \left(\rho_c \tilde{J}_K \right) = \frac{N}{2\tilde{D}} \left(\rho_c \tilde{J}_K \right)^2. \quad (\text{A12})$$

This gives $T_K = D e^{-\frac{2}{N\rho_c \tilde{J}_K}}$, defined such that the effective coupling diverges $\tilde{J}_K \rightarrow \infty$ at $\tilde{D} \searrow T_K$. Note that the perturbative scaling does not depend on M in the one-loop order with respect to J_K .

Appendix B: Bosonic Perron-Frobenius vector without the $SU(N)$ symmetry

1. Anisotropic exchange interaction

The Hamiltonian \mathcal{H} no longer has the $SU(N)$ symmetry in the case where the N -fold degeneracy of the one-particle impurity levels are lifted. In this case, the effective Hamiltonian for the subspace with fixed M impurity-electrons $\mathcal{H}_{\text{eff}}^{\text{ais}}$ can be obtained, extending Eq. (11) as follows. Replacing E_M in the energy denominator in the right-hand side of Eq. (11) by the lowest energy E_M^{min} , and inserting the complete set $|\{\alpha\}\rangle_M$ for impurity states defined in Eq. (A7), it takes the form

$$\mathcal{H}_{\text{eff}}^{\text{ais}} = \sum_{\{\alpha\}} \mathcal{H}_T \frac{1}{E_M^{\text{min}} - (\mathcal{H}_d + \mathcal{H}_c)} \mathcal{H}_T |\{\alpha\}\rangle_{MM} \langle \{\alpha\}|. \quad (\text{B1})$$

In this case, the energy of intermediate state depends on the initial impurity state $\{\alpha\}$. We will use the notation $\mathcal{H}_d |\{\alpha\}\rangle_M = E_M^{\{\alpha\}} |\{\alpha\}\rangle_M$, and E_M^{min} (E_M^{max}) is the lowest (highest) energy in the M impurity-electrons states. Taking only into account the exchange-interaction part of Eq. (B1), we consider a model defined by

$$\begin{aligned} \mathcal{H}_K^{\text{ais}} &\equiv \frac{1}{2} \sum_{mm'} \sum_{\{\alpha\}} \left(J_{m'm}^{\{\alpha\}} a_m^\dagger a_{m'} d_{m'}^\dagger d_m \right. \\ &\quad \left. - \frac{\bar{J}}{N} a_{m'}^\dagger a_m d_{m'}^\dagger d_m \right) |\{\alpha\}\rangle_{MM} \langle \{\alpha\}|, \quad (\text{B2}) \end{aligned}$$

$$\begin{aligned} J_{m'm}^{\{\alpha\}} &\equiv 2 \left(\frac{v^2}{E_M^{\{\alpha\}} - E_M^{\text{min}} + MU + \epsilon_{m'}} \right. \\ &\quad \left. + \frac{v^2}{E_M^{\{\alpha\}} - E_M^{\text{min}} - (M-1)U - \epsilon_m} \right), \quad (\text{B3}) \end{aligned}$$

$$\bar{J} \equiv \frac{1}{\binom{N}{M}} \sum_{\{\alpha\}} \frac{1}{M} \sum_m J_{mm}^{\{\alpha\}} {}_M \langle \{\alpha\} | d_m^\dagger d_m | \{\alpha\} \rangle_M. \quad (\text{B4})$$

Here, \bar{J} is defined such that $\mathcal{H}_K^{\text{ais}}$ becomes traceless,

$$\sum_{\{\alpha\}} \sum_{\{\gamma\}} \langle \{\alpha\}, \{\gamma\} | \mathcal{H}_K^{\text{ais}} | \{\gamma\}, \{\alpha\} \rangle = 0, \quad (\text{B5})$$

$$|\{\gamma\}, \{\alpha\}\rangle \equiv \prod_{i=1}^{N_a} a_{\gamma_i}^\dagger \prod_{j=1}^M d_{\alpha_j}^\dagger |0\rangle, \quad (\text{B6})$$

where $\{\gamma_1, \gamma_2, \dots, \gamma_{N_a}\}$ represents a set of occupied conduction electron levels.

We assume that $M = 1, 2, \dots, N/2$ in the following, as the results for the cases $M > N/2$ can be deduced from those for $M < N/2$ through the particle-hole transform. To be specific, we consider the case where each of ϵ_m 's takes a certain value bounded in the range $\delta\epsilon$ near the middle of the M -electron region Eq. (10),

$$\epsilon_m = - \left(M - \frac{1}{2} \right) U + \delta\epsilon_m, \quad -\frac{\delta\epsilon}{2} < \delta\epsilon_m < \frac{\delta\epsilon}{2}. \quad (\text{B7})$$

We assume that the range $\delta\epsilon$ to be $0 \leq \delta\epsilon < U$. In this case, the exchange coupling is positive $J_{m'm}^{\{\alpha\}} > 0$ for all m, m' , and $\{\alpha\}$. However, this condition is still not sufficient for setting up all the $M \pm 1$ impurity-electrons energies to be much larger than the M impurity-electrons energies. The additional conditions, $E_{M\pm 1}^{\min} - E_M^{\max} \gg 0$, are required:

$$E_{M+1}^{\min} - E_M^{\max} = E_M^{\min} + \frac{U}{2} + \delta\epsilon_{\text{LU}} - E_M^{\max} \gg 0, \quad (\text{B8})$$

$$E_{M-1}^{\min} - E_M^{\max} = E_M^{\min} + \frac{U}{2} - \delta\epsilon_{\text{HO}} - E_M^{\max} \gg 0. \quad (\text{B9})$$

Here, the lowest-unoccupied level $\delta\epsilon_{\text{LU}}$ and the highest-occupied level $\delta\epsilon_{\text{HO}}$ are defined with respect to the lowest M impurity-electrons ground state, and are measured from $-(M-1/2)U$ as Eq. (B7). These two conditions, Eqs. (B8) and (B9), are sufficiently satisfied if the Coulomb repulsion is large much larger than the energy separation between M -electrons impurity states such that

$$\frac{U}{2} \gg \left(M + \frac{1}{2}\right) \delta\epsilon. \quad (\text{B10})$$

Note that the energy separation is bounded in the range $E_M^{\max} - E_M^{\min} < M\delta\epsilon$ by definition given in Eq. (B7).

The lower bound of the exchange interaction can be estimated from Eq. (B3) through the matrix element for which $E_M^{\{\alpha\}} = E_M^{\max}$,

$$\begin{aligned} J_{m'm}^{\{\alpha\}} &> \frac{2v^2}{M\delta\epsilon + \frac{U}{2} + \delta\epsilon_{m'}} + \frac{2v^2}{M\delta\epsilon + \frac{U}{2} - \delta\epsilon_m} \\ &> \frac{4v^2}{\left(M + \frac{1}{2}\right)\delta\epsilon + \frac{U}{2}} = \frac{J_K^0}{1+x}. \end{aligned} \quad (\text{B11})$$

Here, $J_K^0 \equiv 8v^2/U$ and $x = \frac{2\delta\epsilon}{U}(M+1/2)$. Note that $x \ll 1$ from Eq. (B10). Similarly, the upper bound of the exchange interaction is estimated through the matrix element for which $E_M^{\{\alpha\}} = E_M^{\min}$,

$$\begin{aligned} J_{m'm}^{\{\alpha\}} &< \frac{2v^2}{\frac{U}{2} + \delta\epsilon_{m'}} + \frac{2v^2}{\frac{U}{2} - \delta\epsilon_m} \\ &< \frac{8v^2}{U - \delta\epsilon} = \frac{J_K^0}{1 - \frac{x}{2M+1}}. \end{aligned} \quad (\text{B12})$$

This also determines the upper bound of the average \bar{J} , defined in Eq. (B4), as

$$\frac{J_K^0}{1 - \frac{x}{2M+1}} > \bar{J}. \quad (\text{B13})$$

We next consider the following inequality

$$\frac{J_K^0}{1+x} > \frac{J_K^0}{1 - \frac{x}{2M+1}} \frac{M}{N}, \quad (\text{B14})$$

which is satisfied for $0 \leq x \ll 1$, namely in the case where Eq. (B10) holds with $M/N \leq 1/2$. In this case,

we obtain the following relation, using Eqs. (B11), (B13), and (B14),

$$J_{mm'}^{\{\alpha\}} > \frac{\bar{J}M}{N}. \quad (\text{B15})$$

2. Strong exchange coupling limit

The eigenstates of the Hamiltonian $\mathcal{H}_K^{\text{ais}} + \mathcal{H}_d$, which is described in in Eq. (37) with the *hole-picture*, can be expanded using the basis set Eqs. (38) and (39).

As mentioned in Sec. III B, the pair wavefunction $\psi_{\text{pair}}(\{m_p\})$ is an eigenvector of a $\binom{N_{\text{UB}}}{N_{\text{pair}}}$ dimensional Hamiltonian matrix, which has $(N_{\text{UB}} - N_{\text{pair}})N_{\text{pair}}$ *negative* off-diagonal elements, $-J_{m'm}^{\{\alpha\}}/2$, in each column and their Hermitian-conjugate elements in each row. The gain of the *hopping* energy of the pairs is maximized for $N_{\mathcal{O}_d} = N_{\mathcal{O}_h} = 0$, where the pairs are not blocked by the unpaired objects. In this case, the dimension of the subspace becomes largest

$$\binom{N_{\text{UB}}}{N_{\text{pair}}} = \binom{N - N_{\mathcal{O}_d} - N_{\mathcal{O}_h}}{M - N_{\mathcal{O}_d}} \leq \binom{N}{M}, \quad (\text{B16})$$

as the numbers of unpaired objects take values in the range: $N_{\mathcal{O}_d} = 0, 1, \dots, M$ and $N_{\mathcal{O}_h} = 0, 1, \dots, N - M$. Furthermore, the number of the states which are directly linked by the negative off-diagonal elements is maximized

$$\begin{aligned} (N_{\text{UB}} - N_{\text{pair}})N_{\text{pair}} &= (N - M - N_{\mathcal{O}_h})(M - N_{\mathcal{O}_d}) \\ &\leq (N - M)M. \end{aligned} \quad (\text{B17})$$

We next examine the diagonal elements. The diagonal matrix elements of $\mathcal{H}_K^{\text{ais}} + \mathcal{H}_d$ with respect to the basis set Eq. (38), or (39), are determined by the last three terms of Eq. (37),

$$\sum_{m_d \in \mathcal{O}_d}^{N_{\mathcal{O}_d}} \frac{J_{m_d, m_d}^{\{\alpha\}}}{2} - \frac{\bar{J}M[N - (M - N_{\mathcal{O}_d} + N_{\mathcal{O}_h})]}{2N} + E_M^{\{\alpha\}}. \quad (\text{B18})$$

Here, the impurity part $|\{\alpha\}\rangle_M$ contains $N_{\mathcal{O}_d}$ unpaired electrons at $\{m_d\}$ and N_{pair} electrons consisting pairs at $\{m_p\}$. As $\bar{J} > 0$, the diagonal element increases with $N_{\mathcal{O}_h}$, and thus it is minimized at $N_{\mathcal{O}_h} = 0$. In order to minimize the diagonal elements further varying $N_{\mathcal{O}_d}$, we rewrite Eq. (B18) in the following form taking $N_{\mathcal{O}_h} = 0$,

$$\frac{1}{2} \sum_{m_d \in \mathcal{O}_d}^{N_{\mathcal{O}_d}} \left(J_{m_d, m_d}^{\{\alpha\}} - \frac{\bar{J}M}{N} \right) - \frac{\bar{J}M(N - M)}{2N} + E_M^{\{\alpha\}}. \quad (\text{B19})$$

The first term has a lower bound which follows from Eqs. (B10) and (B15),

$$\frac{1}{2} \sum_{m_d \in \mathcal{O}_d}^{N_{\mathcal{O}_d}} \left(J_{m_d, m_d}^{\{\alpha\}} - \frac{\bar{J}M}{N} \right) \geq 0, \quad (\text{B20})$$

where the equality holds at $N_{\mathcal{O}_d} = 0$. Thus, each of the diagonal elements for given $\{\alpha\}$ takes the smallest value for $N_{\mathcal{O}_d} = N_{\mathcal{O}_h} = 0$:

$$-\frac{\bar{J}M(N-M)}{2N} + E_M^{\{\alpha\}}. \quad (\text{B21})$$

Due to these structures of the Hamiltonian matrix, the ground state of $\mathcal{H}_K^{\text{ais}} + \mathcal{H}_d$ is given by the Perron-Frobenius vector for $N_{\mathcal{O}_d} = N_{\mathcal{O}_h} = 0$.

Appendix C: Ward identities

The occupation number of the impurity levels can be written, using the Friedel sum rule given in Eq. (50),

$$\langle n_{d,m} \rangle = \frac{1}{\pi} \cot^{-1} \left[\frac{\epsilon_m + \Sigma_m(0)}{\Delta} \right]. \quad (\text{C1})$$

Taking a derivative with respect to $\epsilon_{m'}$, we obtain,

$$\frac{\partial \langle n_{d,m} \rangle}{\partial \epsilon_{m'}} = -\rho_{d,m}(0) \tilde{\chi}_{mm'}, \quad (\text{C2})$$

$$\tilde{\chi}_{mm'} \equiv \delta_{mm'} + \frac{\partial \Sigma_m(0)}{\partial \epsilon_{m'}}. \quad (\text{C3})$$

The Ward identities relate the derivative of the self-energy to the vertex corrections,⁴⁸ and can be expressed in the following form for the multi-orbital Anderson impurity \mathcal{H} defined in Eqs. (1)–(3),

$$\begin{aligned} & \delta_{mm'} + \frac{\partial \Sigma_m(i\omega)}{\partial \epsilon_{m'}} + \Gamma_{mm':m'm}(i\omega, 0; 0, i\omega) \rho_{d,m'}(0) \\ &= \delta_{mm'} \left(1 - \frac{\partial \Sigma_{m'}(i\omega)}{\partial i\omega} \right). \end{aligned} \quad (\text{C4})$$

At zero frequency $\omega = 0$, this can be rewritten in terms of the enhancement factor $\tilde{\chi}_{mm'}$, defined by Eq. (C3), and the renormalization factor Z_m , as

$$\tilde{\chi}_{mm'} = \frac{1}{Z_m} \delta_{mm'} - \Gamma_{mm':m'm}(0, 0; 0, 0) \rho_{d,m'}(0). \quad (\text{C5})$$

Note that $\Gamma_{mm:mm}(0, 0; 0, 0) = 0$ for $m' = m$. The *Fermi-liquid relations* for the coefficients $\partial \langle n_{d,m} \rangle / \partial \epsilon_{m'}$, given in Eq. (59), follow from this identity and Eq. (C2).

The Ward identity Eq. (C4) can be proved following Yoshimori's Feynman-diagrammatic derivations.⁴⁸ In our purpose, to calculate the derivative of the self-energy with respect to ω , we can shift the frequencies of the propagators along the closed loops of two different groups: one group carrying the external label m and the other group carrying $m' (\neq m)$ chosen from the rest of the orbital indices. The identity in the form Eq. (C4) can also be deduced from a current conservation law, which in the present case corresponds to the local charge conservation in each of the *flavors* “ m ”,

$$\frac{\partial n_{d,m}}{\partial t} + J_m = 0, \quad J_m \equiv iv (d_m^\dagger a_m - a_m^\dagger d_m). \quad (\text{C6})$$

The derivation along this line uses three-point vertex functions of a Ward-Takahashi form^{50,55} and makes it clear the fact that Eq. (C4) is the relation which represents the local charge conservation Eq. (C6).

¹ A. C. Hewson, *The Kondo Problem to Heavy Fermions* (Cambridge University Press, 1993).
² S. Sasaki, S. De Franceschi, J. M. Elzerman, W. G. van der Wiel, M. Eto, S. Tarucha, and L. P. Kouwenhoven, *Nature* **405**, 764 (2000).
³ A. J. Keller, S. Amasha, I. Weymann, C. P. Moca, I. G. Rau, J. A. Katine, H. Shtrikman, G. Zarand, and D. Goldhaber-Gordon, *Nat. Phys.* **10**, 145 (2014).
⁴ P. Jarillo-Herrero, J. Kong, H. S. J. van der Zant, C. Dekker, L. P. Kouwenhoven, and S. De Franceschi, *Nature* **434**, 484 (2005).
⁵ A. Makarovski, A. Zhukov, J. Liu, and G. Finkelstein, *Phys. Rev. B* **75**, 241407 (2007).
⁶ W. Izumida, O. Sakai, and Y. Shimizu, *Journal of the Physical Society of Japan* **67**, 2444 (1998).
⁷ L. Borda, G. Zarand, W. Hofstetter, B. I. Halperin, and J. von Delft, *Phys. Rev. Lett.* **90**, 026602 (2003).
⁸ M.-S. Choi, R. López, and R. Aguado, *Phys. Rev. Lett.* **95**, 067204 (2005).
⁹ J. S. Lim, M.-S. Choi, M. Y. Choi, R. López, and

R. Aguado, *Phys. Rev. B* **74**, 205119 (2006).
¹⁰ C. A. Büsser and G. B. Martins, *Phys. Rev. B* **75**, 045406 (2007).
¹¹ F. B. Anders, D. E. Logan, M. R. Galpin, and G. Finkelstein, *Phys. Rev. Lett.* **100**, 086809 (2008).
¹² M. R. Galpin, F. W. Jayatilaka, D. E. Logan, and F. B. Anders, *Phys. Rev. B* **81**, 075437 (2010).
¹³ D. Mantelli, C. P. Moca, G. Zarand, and M. Grifoni, *Physica E: Low-dimensional Systems and Nanostructures* **77**, 180 (2016).
¹⁴ D. R. Schmid, S. Smirnov, M. Margańska, A. Dirnauichner, P. L. Stiller, M. Grifoni, A. K. Hüttel, and C. Strunk, *Phys. Rev. B* **91**, 155435 (2015).
¹⁵ Y. Nishikawa, O. J. Curtin, A. C. Hewson, D. J. G. Crow, and J. Bauer, *Phys. Rev. B* **93**, 235115 (2016).
¹⁶ M. Ferrier, T. Arakawa, T. Hata, R. Fujiwara, R. Delagrangé, R. Weil, R. Deblock, R. Sakano, A. Oguri, and K. Kobayashi, *Nat. Phys.* **12**, 230 (2016).
¹⁷ E. A. Laird, F. Kuemmeth, G. A. Steele, K. Grove-Rasmussen, J. Nygård, K. Flensberg, and L. P. Kouwen-

- hoven, *Rev. Mod. Phys.* **87**, 703 (2015).
- ¹⁸ W. Izumida, R. Okuyama, and R. Saito, *Phys. Rev. B* **91**, 235442 (2015).
- ¹⁹ M. Ferrier, T. Arakawa, T. Hata, R. Fujiwara, R. Delagrèze, Y. Teratani, R. Sakano, A. Oguri, and K. Kobayashi, unpublished.
- ²⁰ K. G. Wilson, *Rev. Mod. Phys.* **47**, 773 (1975).
- ²¹ H. R. Krishna-murthy, J. W. Wilkins, and K. G. Wilson, *Phys. Rev. B* **21**, 1003 (1980).
- ²² P. Nozières and A. Blandin, *J. Phys. (Paris)* **41**, 193 (1980).
- ²³ O. Parcollet, A. Georges, G. Kotliar, and A. Sengupta, *Phys. Rev. B* **58**, 3794 (1998).
- ²⁴ S. Moriyama, T. Fuse, M. Suzuki, Y. Aoyagi, and K. Ishibashi, *Phys. Rev. Lett.* **94**, 186806 (2005).
- ²⁵ Y. Kuramoto and H. Kojima, *Z. Phys. B* **57**, 95 (1984).
- ²⁶ P. Coleman, *Phys. Rev. B* **29**, 3035 (1984).
- ²⁷ N. Read and D. M. Newns, *J. Phys. C* **16**, 3273 (1983).
- ²⁸ P. Schlottmann, *Z. Phys. B* **51**, 49 (1983).
- ²⁹ N. E. Bickers, *Rev. Mod. Phys.* **59**, 845 (1987).
- ³⁰ K. Yosida and K. Yamada, *Prog. Theor. Phys. Suppl.* **46**, 244 (1970).
- ³¹ K. Yamada, *Prog. Theor. Phys.* **53**, 970 (1975).
- ³² R. Sakano, T. Fujii, and A. Oguri, *Phys. Rev. B* **83**, 075440 (2011).
- ³³ A. Oguri, R. Sakano, and T. Fujii, *Phys. Rev. B* **84**, 113301 (2011).
- ³⁴ A. Oguri, *Phys. Rev. B* **85**, 155404 (2012).
- ³⁵ Y. Nishikawa, D. J. G. Crow, and A. C. Hewson, *Phys. Rev. B* **82**, 245109 (2010).
- ³⁶ P. W. Anderson, *J. Phys. C* **3**, 2436 (1970).
- ³⁷ B. Coqblin and J. R. Schrieffer, *Phys. Rev.* **185**, 847 (1969).
- ³⁸ I. Affleck, *Nucl. Phys. B* **336**, 517 (1990).
- ³⁹ C. Mora, *Phys. Rev. B* **80**, 125304 (2009).
- ⁴⁰ C. Mora, P. Vitushinsky, X. Leyronas, A. A. Clerk, and K. Le Hur, *Phys. Rev. B* **80**, 155322 (2009).
- ⁴¹ P. Nozières, *J. Low Temp. Phys.* **17**, 31 (1974).
- ⁴² H. Georgi, *Lie Algebras in Particle Physics: from Isosopin to Unified Theories* (Westview Press, 1982).
- ⁴³ M. E. Peskin and D. V. Schroeder, *An Introduction to Quantum Field Theory* (Westview Press, 1995).
- ⁴⁴ R. W. Richardson, *Phys. Rev.* **159**, 792 (1967).
- ⁴⁵ J. von Delft and F. Braun, “Quantum mesoscopic phenomena and mesoscopic devices in microelectronics,” (Springer Netherlands, Dordrecht, 2000) pp. 361–370.
- ⁴⁶ H. Tasaki, *Phys. Rev. B* **40**, 9192 (1989).
- ⁴⁷ H. Shiba, *Prog. Theor. Phys.* **54**, 967 (1975).
- ⁴⁸ A. Yoshimori, *Prog. Theor. Phys.* **55**, 67 (1976).
- ⁴⁹ A. C. Hewson, *J. Phys.: Condens. Matter* **13**, 10011 (2001).
- ⁵⁰ A. Oguri, *J. Phys. Soc. Jpn.* **70**, 2666 (2001).
- ⁵¹ A. C. Hewson, A. Oguri, and D. Meyer, *Eur. Phys. J. B* **40**, 177 (2004).
- ⁵² A. Oguri, Y. Nisikawa, and A. C. Hewson, *J. Phys. Soc. Jpn.* **74**, 2554 (2005).
- ⁵³ K. Edwards, A. C. Hewson, and V. Pandis, *Phys. Rev. B* **87**, 165128 (2013).
- ⁵⁴ A. C. Hewson, J. Bauer, and A. Oguri, *J. Phys.: Condens. Matter* **17**, 5413 (2005).
- ⁵⁵ J. Schrieffer, *Theory of Superconductivity*, Advanced Book Program Series (Advanced Book Program, Perseus Books, 1983).